Size-velocity correlations in high order moment methods for polydisperse evaporating sprays: modelling and numerical issues

Aymeric Vié, Frédérique Laurent, Marc Massot

▶ **To cite this version:**

Aymeric Vié, Frédérique Laurent, Marc Massot. Size-velocity correlations in high order moment methods for polydisperse evaporating sprays: modelling and numerical issues. 2011. hal-00626869v1

HAL Id: hal-00626869

https://hal.science/hal-00626869v1

Preprint submitted on 27 Sep 2011 (v1), last revised 6 Aug 2012 (v3)

HAL is a multi-disciplinary open access archive for the deposit and dissemination of scientific research documents, whether they are published or not. The documents may come from teaching and research institutions in France or abroad, or from public or private research centers.

L'archive ouverte pluridisciplinaire **HAL**, est destinée au dépôt et à la diffusion de documents scientifiques de niveau recherche, publiés ou non, émanant des établissements d'enseignement et de recherche français ou étrangers, des laboratoires publics ou privés.

Size-velocity correlations in high order moment methods for polydisperse evaporating sprays: modelling and numerical issues

Aymeric Vié[a,b], Frédérique Laurent[a,b], Marc Massot[a,b,c]

[a] *CNRS, UPR 288, Laboratoire d'Energétique moléculaire et macroscopique, combustion, Grande Voie des Vignes, 92295 Chatenay-Malabry, France*
[b] *Ecole Centrale Paris, Grande Voie des Vignes, 92295 Chatenay-Malabry, France*
[c] *Center for Turbulence Research, Stanford University, California 94305-4035, USA*

Abstract

Kah et al. (2010) recently developed the Eulerian Multi-Size Moment model (EMSM) which tackles the modelling and the numerical aspects for the simulation of polydisperse multiphase flows of a gaseous flow field carrying a disperse liquid phase. Using a moment method, they proposed to reconstruct the number density function (NDF) by Entropy Maximisation , which leads to a unique and realizable NDF. This reconstruction is used to simulate the evaporation process, by an evaluation of the flux of droplet disappearance at zero size and an accurate description of the size shift induced by the evaporation as well as the transport in physical space. Although this method demonstrated its great potential for evaporating polydisperse flows, two issues remain to be addressed. First, the EMSM only considers one velocity for all droplets, thus decoupling size from velocity, which will be to restrictive for distributions with a large size spectrum. In most applications size-conditioned dynamics have to be accounted for. Second, the possibility to have separated dynamics for each size can lead to quasi-monodisperse distributions, which corresponds to a hard limiting case for the entropy maximization algorithm. So the behavior of the entropy maximization needs to be investigated, in order to be able to reproduce a larger subset of the moment space. The aim of this paper is thus twofold. First, the entropy maximization and its related algorithm are enhanced by using a more precise integration method in order to handle NDF close to the frontier of the moment space associated with an adaptive number of parameters to reconstruct the NDF accurately and efficiently, as well as tabulated initial guess to optimize the computational time. Then, a new model called CSVM (Coupled Size-Velocity Moments model) is proposed. Size-velocity correlations are addressed either in the evaporation and drag processes, or in the convective transport. To reach this goal, a reconstruction of the velocity for each size is proposed, using only one additional moment per dimension. This reconstruction is evaluated in evaporation-drag 0D cases, to assess its ability to reproduce both phenomena. To handle the convective transport, a new flux splitting scheme is proposed, based on the underlying kinetic description of the disperse phase. The full strategy is evaluated in 1D and 2D cases and shows the ability of the CSVM and its related algorithms to capture the full physics of polydisperse evaporating sprays with a minimal number of moments.

Key words: Polydisperse sprays, high order moment method, Entropy Maximization, flux splitting, size-velocity correlations

1. Introduction

Multiphase flows occur in several industrial applications, such as internal combustion engine ([1, 2] and references therein), gas turbine [3] or rocket booster [4]. Those applications are linked by the existence of a

Email addresses: aymeric.vie@em2c.ecp.fr (Aymeric Vié), frederique.laurent@em2c.ecp.fr (Frédérique Laurent), marc.massot@em2c.ecp.fr (Marc Massot)

disperse liquid phase, composed of droplets. Simulating this disperse phase accurately becomes crucial, as it highly influences the global behaviour of the full device (consumption, overall power, pollutant emissions...).

The description of a disperse phase may rely on a population balance equation (PBE) on the number density function (NDF), namely the Williams-Boltzmann equation [5, 6]. The PBE describes the time evolution of the NDF in the real space (position) and in the phase space determined by the chosen internal coordinates for the description of the NDF (size, velocity, temperature...). Simulating the PBE can be achieved by using the lagrangian direct simulation Monte-Carlo method (DSMC [7]), which solves lagrangian equations for a large sample of particles, in order to reach converged statistics. This approach is considered as the most accurate, but is very expensive, especially for unsteady flows, and is not well adapted for high performance parallel computing (load balancing [8]) as well as for coupling to the gas phase (interpolations between gas and disperse phases [8]). Its use for industrial applications stays unreachable, even with the great increase in computational resources. Eulerian methods can overcome this problem by not directly solving the PBE on the NDF, but its moments, which are integrated quantities over phase space. In idealized cases of monodisperse distributions, i.e.a unique size for all droplets, the NDF can be easily reconstructed because only two moments are necessary to uniquely determined this NDF. But in the case of polydisperse distributions, a finite moment set has potentially an infinity of admissible NDF reconstructions, which is called the Hausdorff moment problem [9], and the goal is to be able to determine a unique NDF, by imposing additional constraints on the reconstruction.

To account for the size polydispersity, three ways can be envisaged:

1. A size space discretization: the size space can be discretized into intervals called "sections" [10], which leads to a Finite Volume formulation called Multifluid approach in the context of sprays [11].
2. A moment method with continuous reconstruction: a limited set of size moments is used to reconstruct the NDF [12, 13].
3. A quadrature-based moment method : a set of moments is used to build a quadrature approximation of the NDF [14, 15].

Discretizing the size phase space is the simplest way to capture the size polydispersity, but in order to limit diffusion in size space, a high number of sections is needed, increasing the computational cost [16]. Adopting a moment point of view may overcome this problem by transporting only one "fluid" with several moments. This can be done using QMOM (quadrature method of moment [14]) or DQMOM (direct quadrature method of moment [15]). Those approaches are linked by the reconstruction of the NDF : a sum of Diracs delta-functions evolving jointly. The difference lies on the fact that QMOM solves equations on the moment set, whereas DQMOM directly solves the equation on the weight and abscissas of the Dirac δ-functions. Those two methods had shown their great potential for coalescence or breakage, but encounter difficulties for evaporating spray, especially with continuous distributions, due to the disappearance flux of droplets at zero size [17]. Actually, the lower order representation of the QMOM or the DQMOM is not able to reproduce this continuous flux, the disappearance of droplet being possible only when a Dirac delta function reaches the zero abscissa, and leading to singular fluxes.

To solve this intrinsic problem of the representation of the NDF, Kah et al. [2, 13] have proposed a new strategy, called Eulerian Multi-Size Moment model (EMSM), taking advantage of a continuous description of the NDF to determine the flux at zero size, and the evaluation of the shift in size induced by evaporation by a a combined flux/quadrature approach. The reconstruction of the NDF is done by Entropy Maximization (EM, [18]). This is a convex optimization problem with constraints, which admits a unique solution, as long as the moment vector stays in the interior of the moment space [19]. This NDF is used to compute the flux at zero size, and the evaporation is evaluated by means of the zero flux and a quadrature approximation. The great potential of EMSM is demonstrated in [20], where it is shown that the computational time for a equivalent accuracy is clearly an advantage over the Multifluid method.

The evolution in size phase space solved, an important issue to be tackled concerns the numerical scheme used to transport the set of moments in the physical space. In general, a first order Finite Volume scheme is able to transport a set of moments vector, preserving the moment space. But for complex problems, high order methods are needed. As shown in [21], classical high order finite volume numerical schemes cannot guaranty to keep the moments in the interior of the moment space. To overcome this difficulty, a kinetic

scheme adapted to a high number of moments is proposed in [20], which uses a linear reconstruction on the canonical moments, and preserves the realisability of the moment set.

The EMSM associated with a stable and realizable kinetic scheme for the physical transport is a good candidate for the simulation of complex flows. But two important issues still remain unsolved. Firstly, the EMSM uses the same velocity for all droplets, independently of their size. This is quite a strong assumption when drag force is accounted for, as it may generate size-conditionned dynamics. The effect of such an assumption is illustrated on Fig. 1, which consists in the injection of droplet perpendicularly to a gaseous crossflow at constant and uniform velocity. When only one velocity is considered for the whole distribution, only one trajectory can be reproduced. This effect is partially accounted for, using a Multifluid approach with 10 sections, because each section has its proper velocity. But for coarse size discretization, this leads to distinct trajectories separated by vacuum regions, as in Fig. 1. Secondly, the ability to capture separated dynamics depending on the droplet size would generate quasi-monodisperse distributions. Unfortunately, the EMSM and its related EM algorithm cannot reproduce this kind of NDF, which are close to the frontier of the moment space. This would limit the applicability of the EM or at least introduce an error for NDF close to the frontier [13]. This type of highly segregative flows is typical of swirling injection [12] in aeronautical configurations, even if the turbulent mixing tends to generate continuous and regular NDF.

In this work, these two issues are addressed. The entropy maximization and its algorithms are enhanced using adaptive procedures, in terms of integration methods and controlled moments, and tabulated initial guess to decrease the computational cost. A new method is proposed, called Coupled Size-Velocity Moments model (CSVM) that take into account size-velocity correlations by the transport of an additional size-velocity moment for each space dimension, which permits to reconstruct the velocity against size. The evolution in size space for the size moments is done by the determination of the disappearance flux of droplets and a size quadrature approximation. But, contrary to the initial EMSM where the evolution of velocity moments is straightforward due to the a unique velocity for all sizes, the newly introduced size-velocity moments also evolve in size space using both size and velocity reconstructions. The evolution in velocity space due to drag force is done using a CQMOM quadrature [22] coupled to EMSM, which permits to account for the coupled size and velocity evolution, by integrating coupled ordinary differential equations. Using a quadrature approach for the evolution in phase space is important, because complex laws for drag force, evaporation and heating can be easily accounted for, even if we consider simple laws in this work [13]. A numerical kinetic scheme is proposed for the convection in real space, which is based on the flux splitting technique, and preserves the moment space.

The paper is organized as follows. First, the EMSM is described, with its advantages and drawbacks. Then improvements of the EM are described, in order to be able to reproduce all the moment space within a controlled error. The CSVM which takes into account size-velocity correlations is then presented, and the ability to describe the evolution in phase space is analyzed. Concerning the transport in physical space, the flux splitting kinetic scheme is detailed and is evaluated on 1D cases. Finally, an evaluation in 2D complex cases (crossflow and Taylor-Green Vortices) is presented.

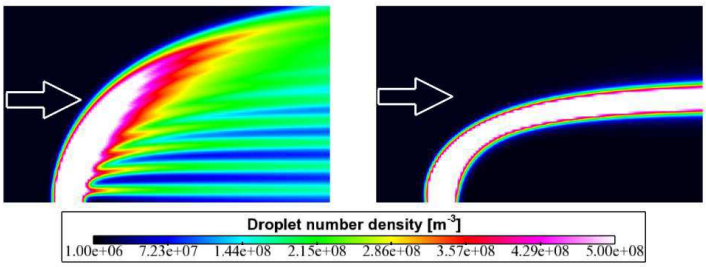

Figure 1: 2D Crossflow: Multifluid method with 10 sections (left) and monodisperse-monokinetic approach (right).

2. The Eulerian Multi-Size Moment model

2.1. The moment problem

Here we consider dilute sprays at high Knudsen number, so that collisions are negligible and there is no effect of the dispersed phase on the gas phase. The phase space of the NDF is limited to size S and velocity v, leading to the following PBE:

$$\frac{\partial f}{\partial t} + v\frac{\partial f}{\partial x} + \frac{\partial}{\partial v}\left(\frac{v-u_g}{\tau_p}f\right) + \frac{\partial R_S f}{\partial S} = 0 \tag{1}$$

where $R_S = dS/dt$ is the evaporation rate which is constant in the case of d^2 evaporation laws and τ_p the relaxation time of the droplets. Using non-dimensional variable $S^* = S/S_{max}$, $t^* = t/\tau_g$, $v^* = v/v_{ref}$ where S_{max} is the maximum droplet surface, τ_g and v_{ref} a reference time scale and velocity of the gaseous flow, we obtain the non-dimensional PBE:

$$\frac{\partial f}{\partial t^*} + v^*\frac{\partial f}{\partial x^*} + \frac{\partial}{\partial v^*}\left(\frac{v^*-u_g^*}{St}f\right) + \frac{\partial R_S^* f}{\partial S^*} = 0 \tag{2}$$

where $\mathrm{St} = \tau_p/\tau_g$ is the Stokes number. For sake of clarity, star exponent will be dropped for non-dimensional variables. To solve this equation, we are looking at the moments of the NDF. In one dimension, these are defined:

$$M_i^l(t,x) = \int_{-\infty}^{\infty}\int_0^1 S^l v^i f(t,x,S)dvdS \tag{3}$$

The equation for $M_i^l(t,x)$ is then:

$$\begin{aligned}\frac{\partial M_i^l}{\partial t} + \frac{\partial M_{i+1}^l}{\partial x} &= -\frac{1}{St}\left(M_i^{l-1} - u_g M_{i-1}^{l-1}\right) \\ &\quad + R_S M_i^{l-1} + R_S\left[\int_{-\infty}^{\infty} v^i S_l f(t,x,v,S)dv\right]_{S=0}^{S=1}\end{aligned} \tag{4}$$

In this equation, the main issues concern the modelling of the second left hand side term (convection) and the third right hand side term (evaporation). The former is due to the fact that with a finite set of moments, the flux for the highest order moment equation is unclosed. The latter imposes the knowledge of point-wise values of the NDF at the edge of the size phase space.

2.2. The moment space

Even if the moment space where lies the size moment vector $\mathcal{M}_0 = (M_0^0, M_0^1, ..., M_0^N)$ is convex, it has a complex geometry in the semi-open space $\mathbb{R}_+^{N+1}$ [13]. The normalized moments vector $(M_0^1/M_0^0, ..., M_0^N/M_0^0)$ lives in a closed convex space of $[0,1]^N$, but still have a complex geometry. A simpler space can be determined by using the canonical moments [19]. The first four canonical moments are:

$$p_0 = 1 \tag{5}$$

$$p_1 = \frac{M_0^1}{M_0^0} \tag{6}$$

$$p_2 = \frac{M_0^0 M_0^2 - {M_0^1}^2}{M_0^1(M_0^0 - M_0^1)} \tag{7}$$

$$p_3 = \frac{(M_0^0 - M_0^1)(M_0^1 M_0^3 - {M_0^2}^2)}{(M_0^0 M_0^2 - {M_0^1}^2)(M_0^1 - M_0^2)} \tag{8}$$

So the actual moments reads:

$$\begin{aligned} M_0^1 &= M_0^0 p_1 && (9)\\ M_0^2 &= M_0^0 p_1 \left[(1-p_1)p_2 + p_1\right] && (10)\\ M_0^3 &= M_0^0 p_1 \left[(1-p_1)(1-p_2)p_2 p_3 + \left[(1-p_1)p_2 + p_1\right]^2\right] && (11) \end{aligned}$$

The canonical moments lie in the $]0,1[^N$, leading to simpler analysis, especially in terms of realisability of the moment vector. The frontier of the moment space is defined by values 0 or 1 for a canonical moment p_k, and implies that canonical moments of order greated than k are not defined. This frontier is characterized by the existence of a unique solution for the NDF, a sum of weighted Dirac δ-functions. In the interior of the moment space where canonical moments are neither equal to 0 nor 1, there is an infinity of NDF, the moments of which are a finite moment vector.

The EMSM tackles the problem of evaporation terms by a reconstruction of the NDF. In this work we will considered 4 moments in size, but the method can be extended to more moments. Considering that each size only have one velocity, the NDF can be decomposed the following way:

$$f(t,x,v,S) = n(t,x,S)\delta(v - U(t,x)) \tag{12}$$

where $U = M_1^0/M_0^0$. The EMSM reconstructs $f(t,x,S)$ using Entropy Maximization (EM, [18]). The Shannon Entropy is defined by:

$$\mathbf{H}(f) = -\int_0^1 f(S)\ln f(S) dS \tag{13}$$

Associated with N moments constraints, the maximization of $\mathbf{H}(f)$ imposes the unique following reconstruction:

$$n_{EM} = \exp\left(-\sum_{j=0}^{N}\zeta_j S^j\right) \tag{14}$$

where ζ_j are Lagrange multipliers. The following convex potential is then minimize:

$$\Delta = \int_0^1 \left[\exp\left(-\sum_{j=0}^{N}\zeta_j S^j\right) - 1\right] dS + \sum_{j=0}^{N}\zeta_j M_0^j \tag{15}$$

The stationary points are given by:

$$\frac{\partial\Delta}{\partial\zeta_i} = 0 \Rightarrow \int_{S_{min}}^{S_{max}} S^i \exp\left(-\sum_{j=0}^{N}\zeta_j S^j\right) dS = M_0^i \tag{16}$$

Numerically, this non-linear system is solved using a Newton method: starting form initial choices $\zeta = (\zeta_0, ..., \zeta_N)^T$, updated ζ is defined from:

$$\zeta^+ = \zeta - H^{-1}(\mathcal{M}_0 - \langle X\rangle_\zeta) \tag{17}$$

where $\langle X\rangle_\zeta = (\langle x^0\rangle_\zeta, ..., \langle x^N\rangle_\zeta)^T$ is the vector of approximated moments:

$$\langle x^i\rangle = \int_0^1 x^i \exp\left(-\sum_{j=0}^{N}\zeta_j S^j\right) dx \tag{18}$$

and H is the Hessian matrix defined by $H_{i,j} = \frac{\partial\Delta}{\partial x_i \partial x_j} = \langle x^{i+j}\rangle_\zeta$. A Gauss-Legendre quadrature method evaluates the integrals. In [13], it has be proven that this integration method with 15 quadrature points is

sufficient to reach the subset $[0.01, 0.99]^3$ of the canonical moment space and that it is sufficient to evaluate the disappearance flux of droplet at zero size within an error less than 1%.

Starting from the reconstructed NDF, The evaluation of the evaporation process is made in two step. First, the disappearance flux at zero size is evaluated, and correspond to the part of the moment that will disappear during a time step Δt:

$$F_i^l = \int_0^{R_S \Delta t} U^i S^l n_l(S) dS \tag{19}$$

corresponding to the part of the distribution which reach the zero size during one time step. The moment are then corrected:

$$\tilde{M}_i^l = M_i^l - F_i^l \tag{20}$$

The evolution in phase space is determined by a quadrature approach:

$$\tilde{M}_i^l = U^i \sum_{k=1}^{2} w_k S_k^l \tag{21}$$

$$\frac{dS_k}{dt} = R_S \tag{22}$$

$$S_k(t + \Delta t) = S_k(t) + R_S \Delta t \tag{23}$$

As stated in [13], this method can account for d^2-law as well as arbitrary evaporation law with a good accuracy.

For the transport in physical space, Kah et al. [20] developed a second order Finite Volume scheme based on a spatial reconstruction of the canonical moments, which preserves the moment space. The authors evaluated the full strategy on complex 2D configurations and had proven its ability to predict such evaporating polydisperse flows, as well as its high efficiency comparing to the Multifluid approach.

3. Numerical issues with Entropy Maximization

In [13], the Entropy Maximization is used to quantify the disappearance flux of droplets. Such an algorithm was design in order to mainly treat smooth distribution where the EM reconstruction associated with a Gauss-Legendre quadrature is able to reach a controlled precision of typically 10^{-6} on the evaporative flux, within the limit of a reasonable number of Newton steps. Even if some treatment was proposed in [13] at the frontier of the moment space the method could only achieve a precision of 10^{-2} in the favorable context of size-velocity decoupling which was coherent with the expected level of modeling of that paper. Unfortunately, in the present context, where we reach a much better precision in terms of size-velocity coupling and treatment of polydispersion, the frontier of the moment space will have a much more important role and we need to upgrade such a ME procedure in both precision and algorithmic efficiency in order to cope up with the increase of modeling level.

Three new ingredients will be introduced in the present section. First, in order to drastically increase the computational efficiency of the ME subroutine, a tabulated initial guess for the Newton solver has been implemented and we provide the key features of such an approach which is used in most of the interior of the moment space, that is in the cube $[0, 1]^3$ in terms of the canonical moments. Second, two ingredients will be added in order to cope with a large subset of the moment space close to the frontier. An adaptive support for the evaluation of the integrals in the ME subroutine has been implemented, thus leading to an important gain in precision. Besides, an adaptive reduction of the number of parameters required for the description of the moments vectors very close to the frontier of the moment space is implemented, which allows to further the same level of precision much closer to the frontier of the moment space that was achieved in [13]. These improvements will prove to be exactly what is needed as far as accurate description of the moment space in order to cope with a precise description of the size-velocity correlations.

3.1. Tabulation

To reduce the number of iterations needed for the Newton solver to converge, the tabulation of all parameters is considered. The evolution of the parameters against canonical moments is first investigated. On Fig. 2, parameters ζ_1, ζ_2 and ζ_3 of the behaviour are plotted against p_2 and p_3 for $p_1 = 0.1, 0.5, 0.9$. Notice that p_2 and p_3 vary between 0.1 and 0.9. Considering the smooth evolution of parameters in the interior of the moment space, the tabulation may give accurate results. The question is now to evaluate the error for a direct tabulation of the parameters.

Two interpolation methods are compared for the tabulation: a linear reconstruction and a third order polynomial reconstruction. The tabulation step is $\Delta p = 0.01$ for each canonical moment, and the tabulation is done in the interval $[0.1, 0.9]^3$.

On Tab. 1, the error made on the moments by the two methods are compared for different sets of canonical moments in the interior of the moment space. Each set is chosen to be as far as possible from tabulated value, to exhibit the maximal error. It can be seen that, even with a third order polynomial the error can be close to 10^{-4}, which can be relatively high as long as this reconstruction is the basis of moment evolution in phase and physical spaces.

p_1	p_2	p_3	Linear	3rd order
0.105	0.105	0.105	3.8e-3	7.0e-5
0.505	0.505	0.505	3.3e-4	2.9e-7
0.895	0.895	0.895	3.7e-3	1.0e-4
0.505	0.105	0.105	4.3e-3	4.8e-5
0.505	0.895	0.895	2.6e-3	7.3e-5

Table 1: Error on moments using a linear or a third order interpolation method for five set of canonical moments.

To reach an acceptable accuracy, it is proposed to use the tabulation to define an initial guess for the Newton iterative solver, which is supposed to reduce the computational time needed to reach a given accuracy of 10^{-6}. On Tab. 2, it can be seen that the tabulation of the initial guess lowers significantly the computational time needed and the number of Newton iterations needed, the fastest method being the more precise third order reconstruction for the initial guess.

p_1	p_2	p_3	Constant	Nearest	Linear	3rd order
0.105	0.105	0.105	1.18s/12it	0.55s/4it	0.33s/2it	0.25s/1it
0.505	0.505	0.505	0.27s/4it	0.18s/2it	0.12s/1it	0.09s/0it
0.895	0.895	0.895	5.13s/17it	0.81s/3it	0.61s/2it	0.43s/1it
0.505	0.105	0.105	1.35s/8it	0.69s/3it	0.52s/2it	0.37s/1it
0.505	0.895	0.895	1.91s/10it	0.69s/3it	0.54s/2it	0.38s/1it

Table 2: Computational time and number of iterations using a constant initial guess, or a tabulated initial guess with nearest, linear or third order interpolation method for five set of canonical moments.

3.2. Dealing with the frontier of the moment space

As stated in the previous section, the parameters λ evolves slowly with the canonical moments in the subspace $[0.1, 0.9]^3$. But close to the frontier, where at least one canonical moment is in $[0.0, 0.1] \cup [0.9, 1.0]$, the variation of λ for a small variation of the canonical moments could be very important. The tabulation technique cannot be used in this part of the moment space. Howerver the initial guess for the Newton solver is chosen to be the closest point in $[0.1, 0.9]^3$. Now being closer to this frontier imposes two constraints on the Newton solver used for EM: NDF become singular, and the determinant of the Jacobian matrix becomes close to zero, leading to ill-conditioned matrices. We thus introduce two strategies to handle the frontier of the moment space: an adaptive support for the integrals and a way to choose the optimal number of entropy maximization parameters.

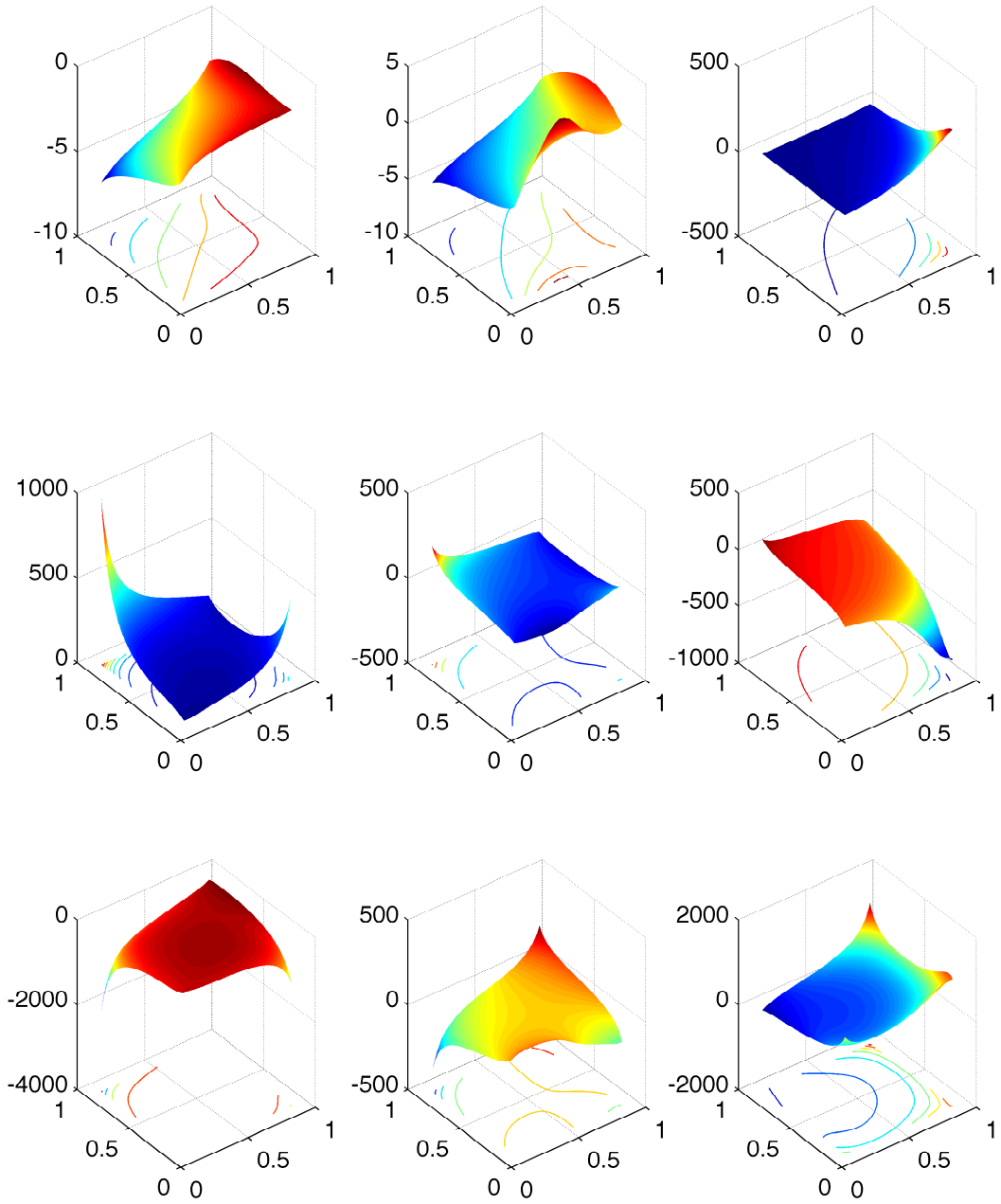

Figure 2: Entropy maximization parameters: ζ_1(up), ζ_2(center) and ζ_3(down) against canonical moments $p_1 = 0.1$ (left), $p_1 = 0.5$ (center), $p_1 = 0.9$ (right).

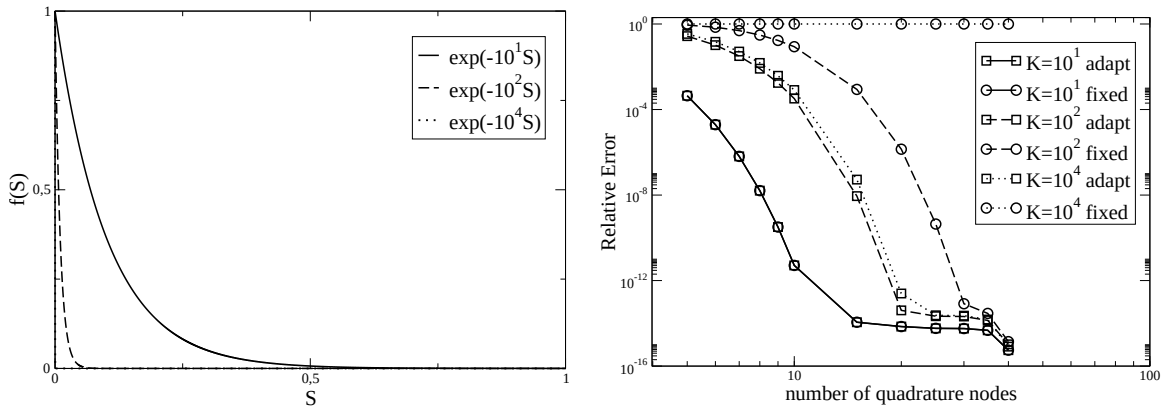

Figure 3: Adaptive integrals: (left) Function $f(S) = \exp(-KS)$ for $K = 10^1$ (full line), $K = 10^2$ (dashed line) and $K = 10^4$ (dot-dashed line) and (right) relative error on the integrals with fixed (circle) and adaptive (square) supports.

3.2.1. Adaptive support for the integrals

The reconstruction can exhibit very high variations for limiting cases near the frontier of the moment space. In such cases, the classical Gauss Legendre quadrature may use abscissas where the function is close to zero, limiting the precision of the method. To overcome this problem, an adaptative support for the gaussian quadrature is proposed. This support is set for a given threshold ϵ_0 in order to locate zones with negligible number density:

$$\exp\left(\sum_{j=0}^{N} \zeta_j S^j\right) = \epsilon_0 \tag{24}$$

$$\sum_{j=0}^{N} \zeta_j S^j - \ln \epsilon_0 = 0 \tag{25}$$

Finding the roots of this polynomial allows to define the integration intervals. As we considered four size moments in this work, the integration support will be made of one or two intervals (as the polynomial will have 3 real roots at most). In practice ϵ_0 is set to the expected tolerance on the integrals evaluation (to reach an accuracy of ϵ on the integrals, ϵ_0 is set to ϵ).

The ability of the adaptive support to compute the integral of singular functions is assessed on the computation of the integral of $\exp(-KS)$ for which the analytical solution is easily found. On Fig. 3, the relative error made by both fixed and adaptive support Gauss Legendre integration methods are shown. For $\exp(-10S)$, the two methods exhibit the same results, as the function extremum on the interval are not so far (1 at $S = 0$ and $\exp(-10) = 4.5.10^{-5}$ at S=1), and the support stays $[0, 1]$ for the adaptive method. For $\exp(-10^2 S)$, the adaptive support is activated, as the extremum values are 1 at $S = 0$ and $\exp(-10^2) = 3.7.10^{-44}$ at S=1. With a threshold at 5.10^{-16}, the adapted support is now $[0, 0.398]$ and the accuracy of the adaptive method is considerably higher, even if the fixed support method is able to compute this integrals with high but reasonable number of nodes. For $\exp(-10^4 S)$, the fixed support method is not able to compute this integral, even with 40 nodes, where the adaptive method uses the support $[0, 4.44.10^{-3}]$ and computes the integral within an error less than 10^{-6} with only 15 nodes, and confirms the importance and the accuracy of the proposed integration method.

3.2.2. Reduction of the number of parameters at the frontier of the moment space

At the frontier of the moment space, the distribution is close to a sum of Dirac δ-functions. For a four-moments reconstruction the two limit cases are a unique δ-function with $S_{dirac} \in]0, 1[$, or two δ-functions at $S = 0$ and $S = 1$, which can be uniquely determined by only two moments. So it appears that close to the

frontier, less moments are needed to capture the NDF. The idea here is to determine where using less than four moments is effective in the sense that we reach the same level of accuracy without leading to unstable numerical methods. The introduced error has to be controlled, as only the border is uniquely determined by less moments.

One can notice that each moment linearly depends on the canonical moment of the same order. So, with respect to p_k, the moment m_k is bounded between $M_0^{k\,min} = M_0^k(p_k = 0)$ and $M_0^{k\,max} = M_0^k(p_k = 1)$. The distance between minimum and maximum values is then:

$$\delta M_0^k = \frac{M_0^k(p_k = 1) - M_0^k(p_k = 0)}{M_0^0} \tag{26}$$

M_0^3 is considered (here the highest order moment):

$$\delta M_0^3 = p_1 p_2 (1 - p_1)(1 - p_2) \tag{27}$$

When this distance is close to 0, the moment M_0^3 weakly depends on p_3, which says that the moment M_0^3 can be accurately reproduced with the first three moments only. The subset where controlling the first three moments is sufficient to achieve an accuracy ϵ_3 on M_0^3 is defined as:

$$p_1 p_2 (1 - p_1)(1 - p_2) < \epsilon_3 \tag{28}$$

Considering $p_1 << 1$ or and when $1 - p_1 << 1$:

$$p_1^{lim,0}(M_0^3) = \frac{\epsilon_3}{p_2(1 - p_2)} \tag{29}$$

$$p_1^{lim,1}(M_0^3) = 1 - \frac{\epsilon_3}{p_2(1 - p_2)} \tag{30}$$

Considering $p_2 << 1$ or and when $1 - p_2 << 1$:

$$p_2^{lim,0}(M_0^3) = \frac{\epsilon_3}{p_1(1 - p_1)} \tag{31}$$

$$p_2^{lim,1}(M_0^3) = 1 - \frac{\epsilon_3}{p_1(1 - p_1)} \tag{32}$$

The minimum (resp. maximum) value of $p_k^{lim,0} = 4\epsilon_3$ (resp. $p_k^{lim,1} = 1 - 4\epsilon_3$) is reached at $p_k = 0.5$. So to achieve an accuracy of ϵ_3 on M_0^3 with only the first three moments, p_1 and p_2 must stay in $[4\epsilon_3, 1 - 4\epsilon_3]$, this condition being less and less restrictive as p_1 and p_2 are conjointly close to the frontier.

The same procedure can be applied to reduce from 3 to 2 moments using the normalized distance for M_0^2:

$$\delta M_0^2 = p_1(1 - p_1) \tag{33}$$

So for a given threshold ϵ_2, using the same method as for δM_0^3, the limits for p_1 are:

$$\delta M_0^2 = p_1(1 - p_1) < \epsilon_2 \tag{34}$$

$$p_1^{lim,0}(M_0^2) = \epsilon_2 \tag{35}$$

$$p_1^{lim,1}(M_0^2) = 1 - \epsilon_2 \tag{36}$$

3.3. Conclusions on the entropy maximization

The proposed adaptive support for integrals enables the accurate computation of the integrals of singular NDF. With the knowledge of the canonical moments, we are now able to choose an optimal initial guess for the Newton solver by means of a tabulation. The number of moments used for the reconstruction can be reduced where less moments are needed. This reduction is limited to a subspace close to the frontier, and we are able to define precisely the error made by this reduction of parameter.

So the EM is now able to reproduce a large subset of the moment space, and is ready for highly segregative case like the crossflow (Fig. 1), where the drag force separates the droplets into quasi-monodisperse NDF, which lie at the frontier of the moment space.

4. Accounting for size-velocity correlation: the CSVM method

4.1. Description of the problem

The initial EMSM considers a unique velocity for all sizes. In moderate to high Stokes flows, the velocity of each size would be different, as exhibited in Fig. 1 in the crossflow configuration. So the NDF now writes:

$$f(t,x,v,S) = n(t,x,S)\delta(v - U(t,x,S)) \tag{37}$$

where U depends on position and time, but also on droplet surface. To describe this velocity distribution, a reconstruction strategy is proposed. The starting point is the same as the initial EMSM for the reconstruction of the size distribution: with a certain number of moments, we need to have an accurate enough description of the NDF. As we want to build size-velocity informations, size-velocity moments will be used:

$$M_i^l = \int_0^1 S^l U(S)^i n(S) dS \tag{38}$$

So that the CSVM will use size moments to determine the size distribution $n(S)$ and size-velocity moments to determine $U(S)$. As the determination of $n(S)$ does not need $U(S)$ (size moments does not depend on $U(S)$), this first step of the EMSM is unchanged. However the velocity reconstruction depends on the size reconstruction.

4.2. Strategy for the velocity reconstruction

Hereafter, the reconstruction strategy for one dimension is proposed. The application for others directions is straightforward, as the used size-velocity moments will be at first order in velocity ($i = 1$).

To evaluate the velocity of each size, a reconstruction shape of $U(t,x,S)$ is proposed. A constraint on this reconstruction is that droplets with a null size and so a null relaxation time follow the gas phase:

$$U(t,x,S=0) = u_g \tag{39}$$

To be able to represent all possible moment vectors, it is necessary to propose a reconstruction that can describe the full velocity moment space. The following power reconstruction is proposed:

$$U(t,x,S) = u_g + \sum_{k=1}^{N} A_k S^{\alpha_k} \tag{40}$$

Where A_k are the parameters used to control the size-velocity moments, and α_k are user-determined with $\alpha_1 < \alpha_2 < ... < \alpha_N$. Considering size-velocity moments expression, one can write:

$$M_1^l = M_0^l u_g + \sum_{k=1}^{N} A_k \int_0^1 S^{\alpha_k + l} n_l(S) dS \tag{41}$$

which gives the linear system for the parameters vector $\mathcal{A}$:

$$M\mathcal{A} = \mathcal{N} \tag{42}$$

where:

$$\begin{aligned} M_{kl} &= \int_0^1 S^{\alpha_k + l} n_l(S) dS \\ N_l &= M_1^l - M_0^l u_g \end{aligned}$$

Considering the linear system, the only configuration for which this reconstruction will not be possible for a given moment corresponds to the zero determinant for matrix M_{kl}. In practice, this condition is reached

for Dirac's delta function for the size distribution $n(S)$. As the EM will never reach this type of distribution (the EM can be as close as possible but never reach the frontier of the moment space), it is emphasized that this reconstruction will be able to reproduce any moment set that will be generated by the EMSM.

In [12], an exponential reconstruction is proposed, based on the analytical solution of the relaxation of droplets at constant gas velocity. Although this is a physical and relatively smooth reconstruction, with good asymptotic predictions, this shape is not able to reproduce all the moment space, as it cannot capture inversions in the relative velocity between gas and droplets, which is a typical case with oscillating gas velocity. In this work, as the aim is to design a method with as few moments as possible, only one additional size-velocity moment per dimension will be used, compared to the original EMSM.

4.3. Evaluation of the proposed strategy

To evaluate the proposed reconstruction, a 0D analytical test case is proposed, in which a initial size-velocity distribution evolves because of the drag force imposed by a constant gas velocity. The initial size and velocity distributions are constant so that $n(S,t) = 1$ and $U(S, t = 0) = U^0$. For each size, this case is solution of the ordinary differential equation:

$$\frac{dU(S,t)}{dt} = F_d = -\frac{U(S,t) - u_g}{St(S)} \tag{43}$$

so:

$$U(S,t) = u_g + (U^0 - u_g)\exp\left(-\frac{t}{St(S)}\right) \tag{44}$$

The moments evolution against time is:

$$\begin{aligned} M_1^l(t) &= \int_0^1 S^l U(S,t) n(S) dS = \frac{u_g}{l+1} + (U^0 - u_g)\int_0^1 S^l \exp\left(-\frac{t}{St(S)}\right) dS \\ M_1^0(t) &= u_g + \frac{t}{K_d}(U^0 - u_g)\Gamma_{inc}\left(-1, \frac{t}{K_d}\right) \text{ if } t > 0 \qquad (45) \\ M_1^1(t) &= \frac{u_g}{2} + \frac{t^2}{K_d^2}(U^0 - u_g)\Gamma_{inc}\left(-2, \frac{t}{K_d}\right) \text{ if } t > 0 \qquad (46) \end{aligned}$$

where $\Gamma_{inc}(a,z) = \int_z^\infty x^{a-1}\exp(-x)dx$ is the upper incomplete gamma function and $St(S) = K_d S$, which corresponds to Stokes drag.

On Fig. 4, the influence of the power α_1 and α_2 on the absolute reconstruction error in L^∞ norm is shown for $t = 1$. Two optimal zones are exhibited, the first one with high powers nearly identical, and the second one with one power close to 1 and the second one less than 1. In Practice, $\alpha_1 = 0.5$ and $\alpha_2 = 1$ will be used.

Results are plotted on Fig. 5. For a two parameters reconstruction, it proves to be efficient except for a constant velocity distribution. This error may be reduced by using more moments.

A second analytical test case is proposed, with variable gas velocity $u_g = \alpha\cos(\beta t)$. It aims at representing the velocity profile inside a vortex, and so the effect of a turbulent structure. The solution of Eq. 43 is then:

$$U(S,t) = \frac{\alpha\left(\beta St\sin(\beta t) + \cos(\beta t)\right)}{\beta^2 St^2 + 1} + \frac{\left[U^0\beta^2 St^2 + (U^0 - \alpha)\right]\exp(-\frac{t}{St})}{\beta^2 St^2 + 1} \tag{47}$$

Results are plotted on Fig.6. Again the reconstruction is satisfactory with only two moments and so two parameters, and proves to be able to reproduce distributions with an inversion of the gas relative velocity, which would be typical of turbulent flow with a wide spectrum of droplet sizes. Furthermore, as a relative velocity inversion occurs, an exponential function would not be able to reproduce such a distribution.

So we are able to reconstruct the droplet number density as well as the velocity for each size. Now, we need to predict the evolution of this NDF through evaporation, drag force and convection.

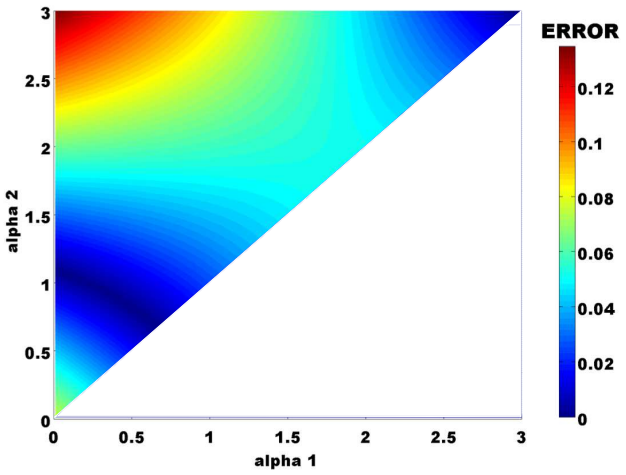

Figure 4: CSVM reconstruction error for the 0D test case at constant gas velocity for $t = 1$ against α_1 and α_2. For $\alpha_2 < \alpha_1$ the error is not plotted. For $\alpha_1 = \alpha_2$, the reconstruction is undefined.

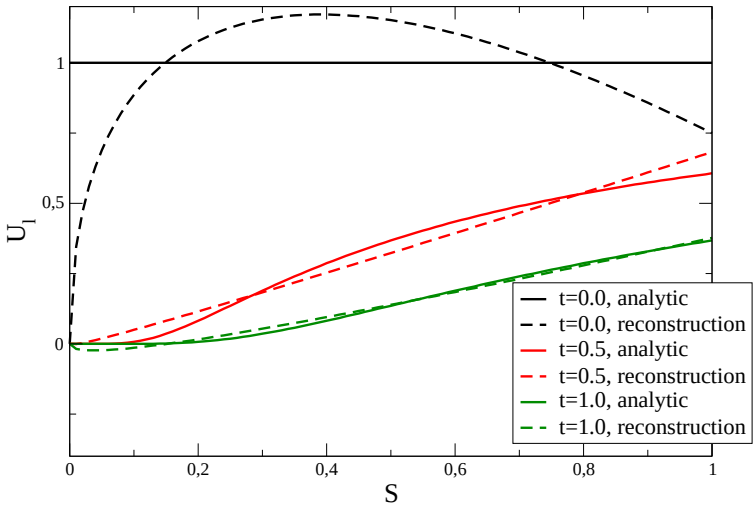

Figure 5: 0D analytical test case with constant gas velocity: velocity distribution (solid lines) and its reconstruction by CSVM (dashed lines).

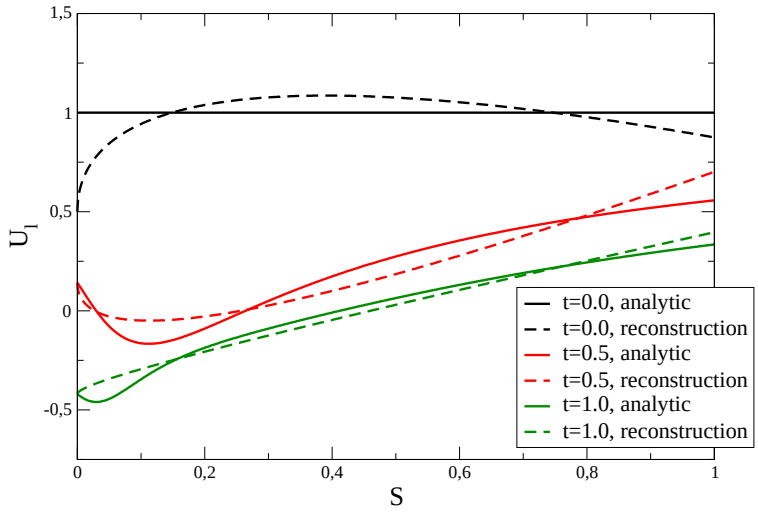

Figure 6: 0D analytical test case with sinusoidal gas velocity: velocity distribution (solid lines) and its reconstruction by CSVM (dashed lines).

5. Numerical methods for the moment evolution

5.1. Evaporation and drag force

5.1.1. Description of the proposed strategy

Here the evolution of the NDF through evaporation and drag force is proposed. The method described in [13] is based on two main steps: the evaluation of the disappearance flux of droplet, and the evolution in size space. Here the strategy is extended to the evolution in velocity space through drag force. First the derivation is shown for d^2 law and Stokes drag ($R_S = cte$ and $St(S) = K_d S$). The size reconstruction of the CSVM enables the computation of the disappearance flux of droplet F_i^l for each moment and for one time step Δt:

$$F_i^l = \int_0^{-R_S \Delta t} U(S)^i S^l n_l(S) dS \tag{48}$$

corresponding to the part of the distribution which reaches the zero size during one time step. The moment are then corrected:

$$\tilde{M}_i^l = M_i^l - F_i^l \tag{49}$$

The evolution in phase space is determined by the CQMOM quadrature approach [22] :

$$\tilde{M}_i^l = \sum_{k=1}^{2} w_k S_k^l U_k^i \tag{50}$$

$$\frac{dU_k}{dt} = -\frac{1}{St}(U_k - u_g) = -\frac{1}{K_d S_k}(U_k - u_g) \tag{51}$$

$$\frac{dS_k}{dt} = R_S \tag{52}$$

With the ODE in velocity and size, it is then possible to account for most evaporation laws, as stated in [13]. The size and velocity after one time step is:

$$S_k(t + \Delta t) = S_k(t) + R_S.\Delta t \tag{53}$$

$$U_k(t + \Delta t) = (U_k(t) - u_g)\left(\frac{S_k(t) + R_S \Delta t}{S_k(t)}\right)^{\frac{-1}{K_d R_S}} + u_g \tag{54}$$

With the updated quadrature, the new moments can be computed.

$$M_i^l(t+\Delta t) = \sum_{k=1}^{2} w_k(t) S_k(t+\Delta t)^l U_k(t+\Delta t)^i \tag{55}$$

To account for complex law, the strategy is slightly modified, the two differences lying on the flux determination and the ODE system that is needed to be solved. Considering $R_S = f(S)$ and $St(S) = g(S)$, the evaluation of the disappearance flux of droplets is now:

$$F_i^l = \int_0^{S_{lim}} U(S)^i S^l n_l(S) dS \tag{56}$$

where S_{lim} is obtained by solving the non-linear system:

$$\begin{cases} \dfrac{dS_{lim}}{dt} = -R_S(S_{lim}) \\ S_{lim}(t = \Delta t) = 0 \end{cases} \tag{57}$$

which means that S_{lim} is the biggest size that reaches the zero size during one timestep. Using this flux, the corrected moments are computed and the quadrature is performed, like with simple laws. Then, the obtain system of ODE cannot be solved analytically:

$$\begin{cases} \dfrac{dU_k}{dt} = -\dfrac{1}{St(S)} \left(U_k - u_g\right) \\ \dfrac{dS_k}{dt} = R_S(S) \end{cases} \tag{58}$$

so an ODE solver is needed. Solving this system of ODE finally gives the new moments, like with simple laws.

5.1.2. Evaluation in 0D test cases

0D test cases are used to evaluate the ability of the CSVM to account for both drag and evaporation. For all cases, the initial liquid velocity distribution is constant and set to 1. The initial size distribution is a normal distribution $n(S) = 1/(\sqrt{2\pi}\sigma).\exp(-(S-\mu)/2\sigma^2)$ with $\sigma = 0.4$ and $\mu = 0.6$. The Stokes number at $S = 1$ is set to 1. Then the test cases are defined by two parameters: the gas velocity against time, $u_g(t)$, and the evaporation rate R_S.

The Lagrangian reference is computed using a tracking of 10^6 particles randomly chosen to fullfill the normal distribution $n(S)$. Eulerian quantities for the reference solution are obtained by projection of the lagrangian particles over the Eulerian grid.

The combined effect of drag force and evaporation is evaluated. Evaporation is the first motivation of the EMSM, and its accuracy has already been demonstrated in [13]. The novelty of this work is the ability to achieve a good accuracy on size-velocity moments. Here we consider $R_S = 1$ and $u_g = 0.5\cos(10t)$.

The evolution of moments against time for lagrangian, CSVM and EMSM are plotted on Fig. 7. For size moments, the results are the same for CSVM and EMSM, as the size reconstruction is still the same. For size-velocity moments, results are better for the CSVM. This result is confirmed by Fig. 8, on which the error for size and size-velocity moments is plotted. For the CSVM, the error is under 3% where it reaches 10% without velocity reconstruction, and this with only one additional moment.

To investigate the ability of the proposed method to capture a more complex dynamic, this test case will consider no evaporation ($R_S = 0$) and a variable gas velocity with three modes, plotted on Fig. 9:

$$u_g(t) = \frac{1}{2}\cos(4\pi t) \text{ if } t \leq 1 \tag{59}$$

$$= \cos(\pi t) \text{ if } 1 < t \leq 5 \tag{60}$$

$$= \frac{1}{4}\cos(8\pi t) \text{ if } t > 5 \tag{61}$$

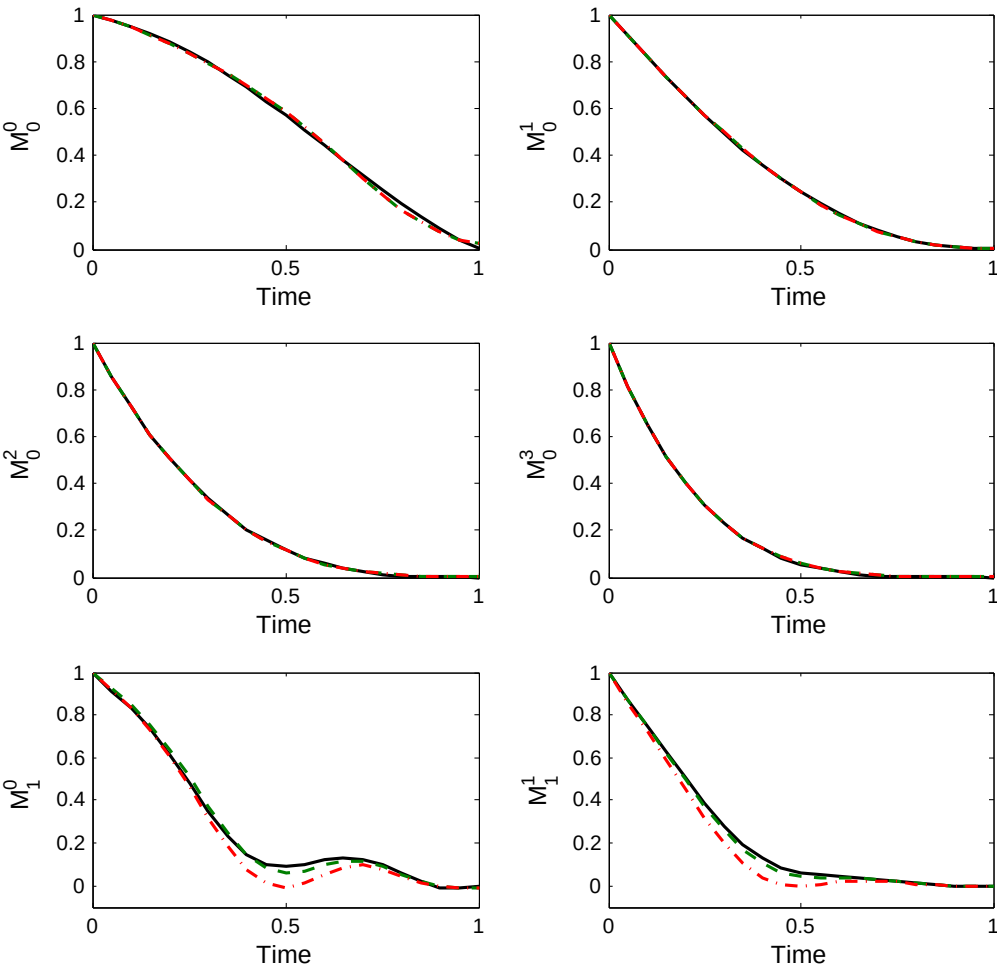

Figure 7: Evolution of moments: lagrangian reference (solid line), CSVM (dashed line), and EMSM (dot-dashed line).

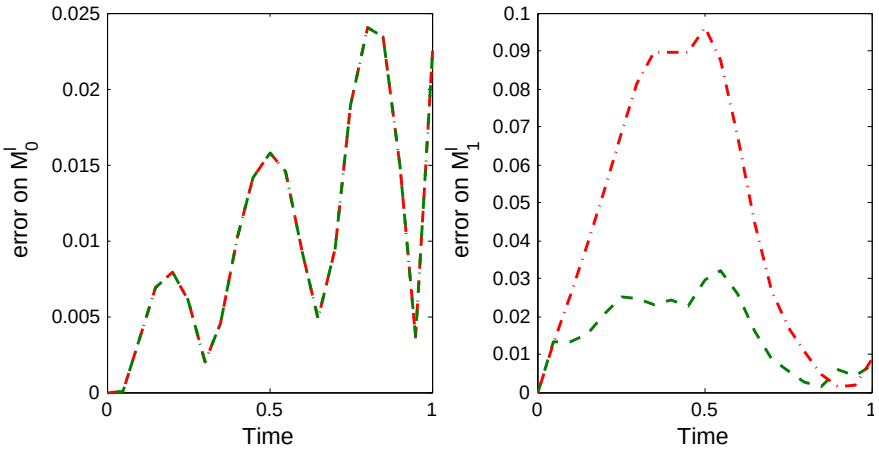

Figure 8: Absolute L^∞ error on size (left) an size-velocity moment (right) vectors comparing to the lagrangian reference: CSVM (dashed line), and EMSM (dot-dashed line) for size moments (left) and size-velocity moments (right).

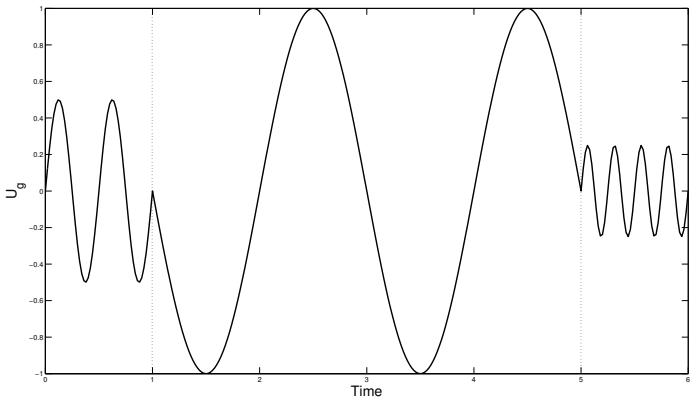

Figure 9: Evolution of the gas velocity against time.

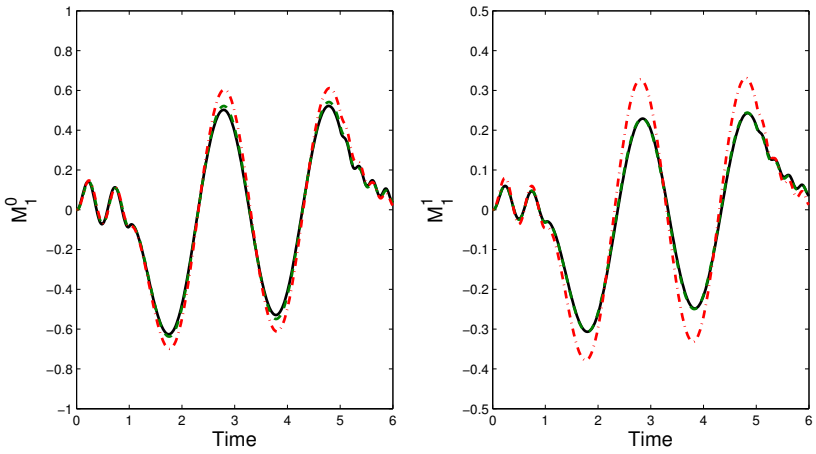

Figure 10: Evolution of moments: lagrangian reference (solid line), CSVM (dashed line), and EMSM (dot-dashed line).

These three modes are expected to mimic what can be seen by particles going through several vortices with different properties. On Fig. 10, the evolution of size-velocity moments against time for CSVM and EMSM. The improvement of the velocity reconstruction is obvious, the error on M_1^1 being invisible with velocity reconstruction. These results are confirmed again by the error on Fig. 11, which stays under 2% with reconstruction and reaches more than 10% without.

Finally, it can be said that CSVM is able to capture the phase space evolution of an evaporating and/or drag forced disperse phase, which is achieve using only one additional moment comparing to the EMSM.

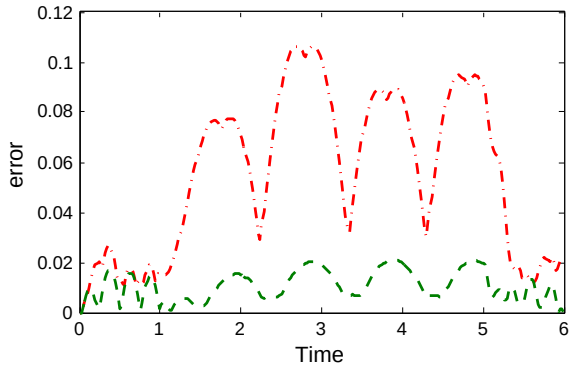

Figure 11: Absolute L^∞ error on size-velocity moments vector comparing to the lagrangian reference: CSVM (dashed line), and EMSM (dot-dashed line).

5.2. Convection scheme

The physical space evolution is surely the most important part of the size-velocity correlation. As seen in previous section, the constant velocity assumption, even if it leads to higher errors, does not lead to a completely different moment evolution in the velocity phase space. But in physical space, as shown by Fig. 1, the dynamics will be totally different. The moment equation for the transport in physical space in one dimension is:

$$\frac{\partial \mathcal{M}}{\partial t} + \frac{\partial \mathcal{F}(\mathcal{M})}{\partial x} = 0 \tag{62}$$

where $\mathcal{M} = (M_0^0, M_0^1, M_0^2, M_0^3, M_1^0, M_1^1)^T$ is the moment vector and $\mathcal{F}(\mathcal{M}) = (M_1^0, M_1^1, M_1^2, M_1^3, M_2^0, M_2^1)^T$ is the flux vector. For a constant velocity distribution, the fluxes are linear functions of the moments ($\mathcal{F}(\mathcal{M}) = U\mathcal{M}$). In this case, a first order finite-volume scheme preserves the moment space, as it is positive definite and the scheme reconstruction generates realizable moments. The second-order scheme that preserves the moment space is much more difficult to design, and this issue raised in the literature [23] had been finally tackled in [20]. In the case of a continuous non-constant velocity, fluxes are now a complex function of the moments, and designing a specific scheme becomes necessary.

5.2.1. Flux splitting kinetic scheme

The moment equation is related to the following kinetic equation:

$$\frac{\partial f}{\partial t} + v_m \frac{\partial f}{\partial x_m} = 0 \tag{63}$$

where $f(t, x, v, S) = n(t, x, S)\delta(v - U(t, x, S))$. Integrating over velocities but not over sizes, the following infinite system for $S = [0, 1]$ is found:

$$\begin{aligned} \frac{\partial n(S)}{\partial t} + \frac{\partial n(S)U(S)}{\partial x} &= 0 \\ \frac{\partial n(S)U(S)}{\partial t} + \frac{\partial n(S)U(S)^2}{\partial x} &= 0 \end{aligned} \tag{64}$$

To solve this system, a first order upwind finite volume scheme is used:

$$n_j^{n+1} = n_j^n - \frac{\Delta t}{\Delta x}\left(F_{j+1/2} - F_{j-1/2}\right) \tag{65}$$

$$n_j^{n+1}U_j^{n+1} = n_j^n U_j^n - \frac{\Delta t}{\Delta x}\left(G_{j+1/2} - G_{j-1/2}\right) \tag{66}$$

where:

$$F_{j+1/2} = \min(0, U^n_{j+1}) n^n_{j+1} + \max(0, U^n_j) n^n_j \quad (67)$$

$$G_{j+1/2} = \min(0, U^n_{j+1}) n^n_{j+1} U^n_{j+1} + \max(0, U^n_j) n^n_j U^n_j \quad (68)$$

By integrating over size, the following scheme is obtained:

$$\mathcal{M}^{n+1}_j = \mathcal{M}^n_j - \frac{\Delta t}{\Delta x} \left(\mathcal{F}_{j+1/2} - \mathcal{F}_{j-1/2} \right) \quad (69)$$

where the fluxes are splitted into positive and negative components:

$$\mathcal{F}_{j+1/2} = \int_0^1 \mathcal{S} \left(\min(0, U^n_{j+1}) n_{j+1} \mathcal{U}^n_{j+1} + \max(0, U^n_j) n_j \mathcal{U}^n_j \right) dS = \mathcal{F}^-_{j+1} + \mathcal{F}^+_j \quad (70)$$

where $\mathcal{S} = [1, S, S^2, S^3, 1, S]^T$ and $\mathcal{U}^n_j = [1, 1, 1, 1, U^n_j, U^n_j]^T$. Using the size and velocity reconstructions these fluxes can be computed for every moments using the adaptive integration method proposed for the EM. To ensure the stability of the scheme, a CFL condition is imposed on the timestep which is also based on the velocity reconstruction:

$$\Delta t < \mathrm{CFL} \frac{\Delta x}{max_S(|U(S)|)} \quad (71)$$

5.2.2. 1D case

The proposed scheme is evaluated on a 1D test case. The spatial distribution is gaussian, the NDF is constant in size, and the velocity is linear in size:

$$n(t = 0, x, S) = \exp\left(-\frac{(x - x_c)^2}{\sigma^2} \right) \quad (72)$$

$$U(t = 0, x, S) = U_g + (U(S = 1) - U_g) S \quad (73)$$

Here $x_c = 0.2$, $\sigma = 0.05$, $U_g = 0$, $U(S = 1) = 1$. The analytical solution for M^0_0 at time $t = 0.6$ is:

$$M^0_0(x, t) = \frac{\sigma \sqrt{\pi}}{2t(U(S = 1) - U_g)} \left[\mathrm{erf}\left(\frac{(U(S = 1)t + x_c - x}{\sigma} \right) - \mathrm{erf}\left(\frac{U_g t + x_c - x}{\sigma} \right) \right] \quad (74)$$

Results are plotted on Fig. 12. The total droplet number is spread by the velocity distribution, and the agreement between analytical and CSVM solutions is satisfactory. The order of the scheme is close to 1, and the method converges to the analytical solution.

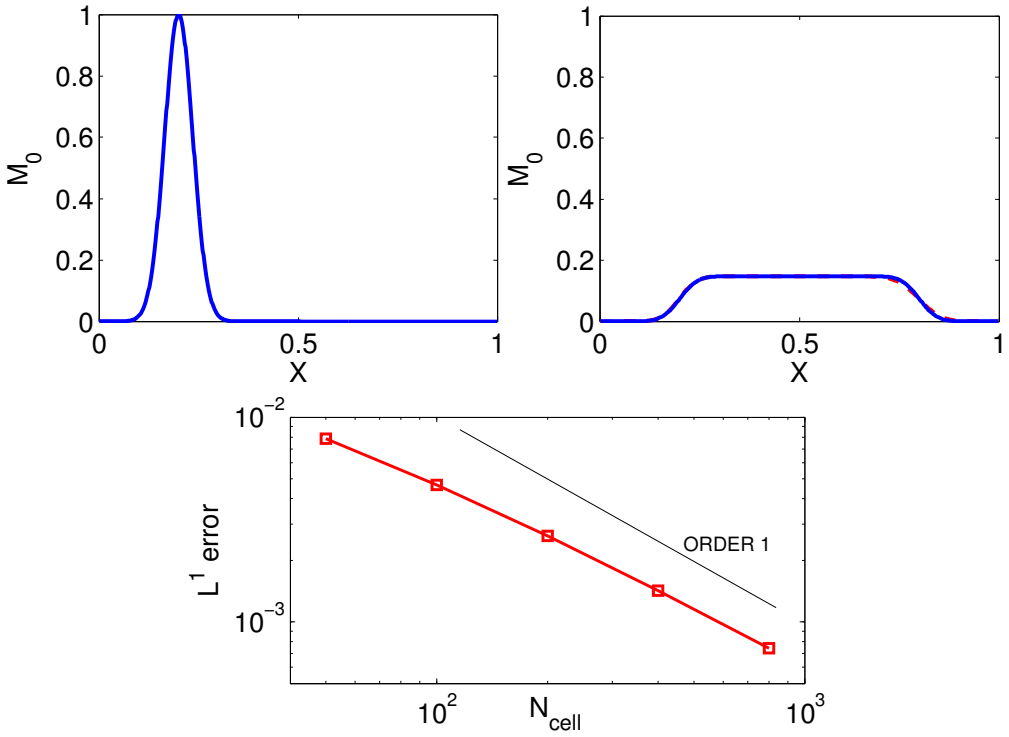

Figure 12: 1D test case: initial total droplet number distribution (upper left), analytical solution at $t = 0.6$ (upper right, full line), CSVM solution at $t = 0.6$ for 400 cells (upper right, dashed line), absolute error against cell number (down).

6. Application to complex cases

Two 2D complex cases are investigated: the crossflow and the Taylor-Green vortices. The first one consists in the injection of particles in the normal direction of a constant gas flow, which leads to a high size segregation and exhibits a steady solution. The second one consists in four contra-rotating vortices in a periodic domain. This case also leads to a high size segregation, but is more complicated as the gas velocity is not constant and imposes that there is no steady solution here. Those two test cases are set to evaluate the proposed method to capture limiting case, i.e. where all moment sets in the domain tends to the frontier of the moment space. In practical applications, NDF tend to continuous and smooth distributions because of the turbulent mixing for example(see [24]). As our analysis will be focused on the dynamics of a polydisperse cloud of droplets, these test cases are non-evaporating.

6.1. Crossflow

The crossflow generates monodisperse distributions due to drag force size-conditioned segregration. As monodiperse distribution are at the frontier of the moment space, it is an interesting case to confirm the ability of the EM to capture such distributions. Moreover considering that every size has its proper velocity and trajectory, it is also a good case for evaluating the transport scheme.

The size of the computational domain is 2 in x direction and 1 in y direction. The injection is made between $X_L = 0.1$ and $X_R = 0.3$, at a constant velocity $V_0 = 1$ and $U_0 = 0$, with a constant number distribution $n(t, x, S) = 1$. The gas flow is constant, at $U_g = 1$ and $V_g = 0$. The semi-analytical solution is described in Appendix 8.B.

On Fig. 13, the droplet number density is shown for the Multifluid approach with 10 and 40 sections, and the CSVM with 4 moments in size and 2 moments in size-velocity. The Multifluid approach considers only one Stokes number for each section, so each section will have only one dynamics, even if the section covers a wide spectrum of Stokes numbers. The effect of such a size discretization is strong with 10 sections (30 moments, 10 in size, 2×10 in velocity), with 10 distinct trajectories. This effect is invisible with 40 sections (120 moments). With the CSVM, as the whole spectrum of Stokes number in the distribution is considered, a continuous number density distribution is obtained. And this is done with only 8 moments.

On Fig. 14, Multifluid approach with 10 and 40 sections, CSVM and analytical solution for the number density distribution and mean surface against Y are compared at the right outlet of the domain. The highly oscillatory behavior of the 10 sections Multifluid solution is exhibited. The 40 sections Multifluid solution is in good agreement with the analytical solution. The CSVM captures a continuous distribution, but exhibits a large scale oscillation. In fact the results are encouraging for a 8 moments solution (to compared with the 30 and 120 moments for Multifluid solution). The quality of the dynamical structure of the solution is confirmed by the mean size. All the method captures relatively well the size distribution, with the worse results for the 10 sections Multifluid and better results for the 40 sections Multifluid. This test case also demonstrates the ability and the robustness of the CSVM to capture high segregation effects with a limited number of moments.

6.2. Taylor Green vortices

The Taylor Green vortices case is more complex than the Crossflow, as it is an unsteady configuration. The segregation effect is strong, small droplet being captured by the vortices, whereas big droplets can move from one to another. Furthermore, droplets with a Stokes number higher than the critical Stokes number $St_c = 1/8\pi$ can exhibit trajectory crossings, and thus a monokinetic eulerian approach (one velocity per size in this work) can generate δ-shock as the system is weakly hyperbolic [25, 26]. The corresponding behaviour is analysed in Appendix 8.A.

The computational domain is 1-by-1 and periodic in each direction. The gas velocity is:

$$U_g(X, Y) = \quad cos(2\pi X)sin(2\pi Y) \tag{75}$$

$$V_g(X, Y) = - \; sin(2\pi X)cos(2\pi Y) \tag{76}$$

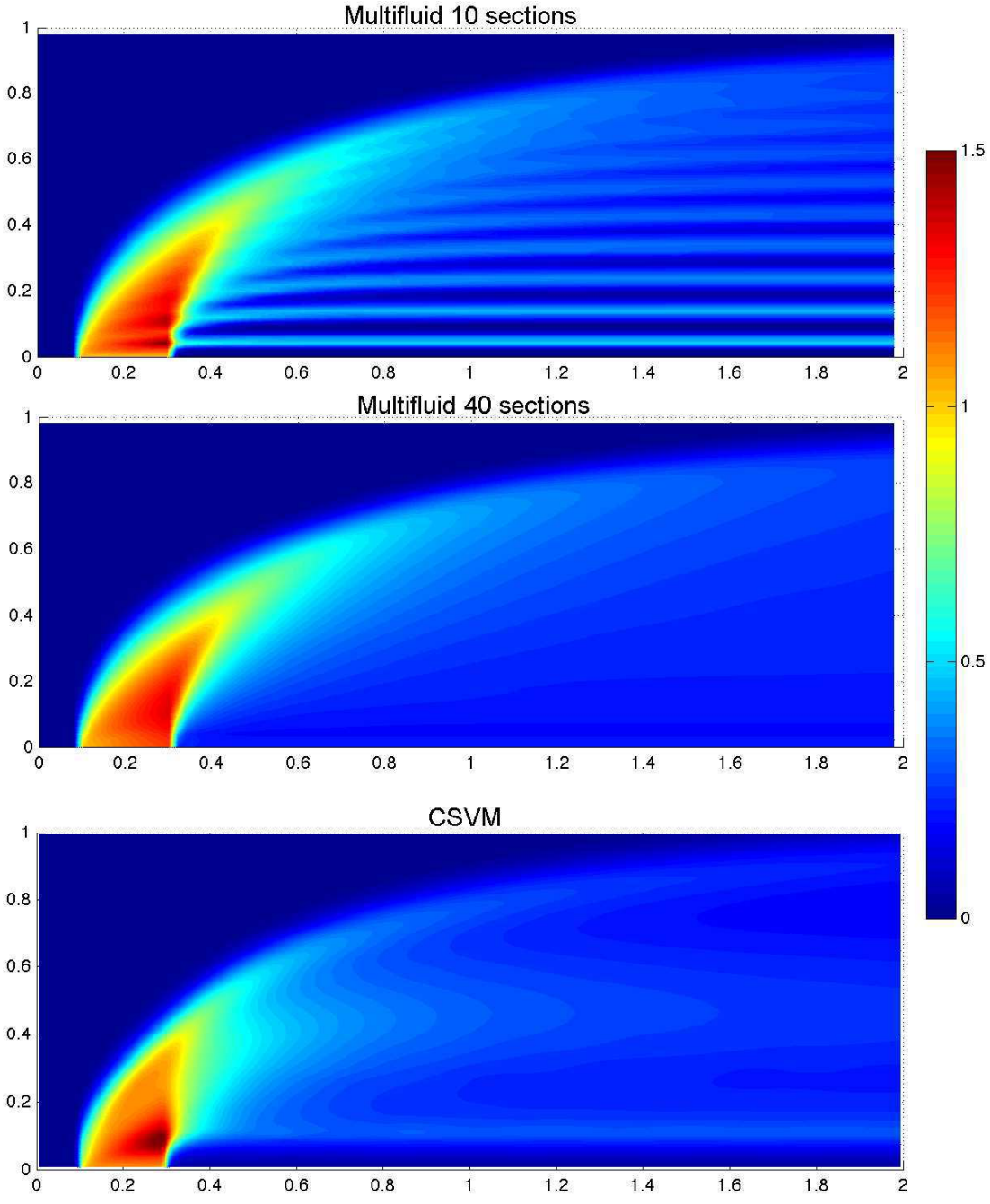

Figure 13: 2D Crossflow: droplet number density for the Multifluid approach with 10 sections (up) and 40 sections (center), and for the CSVM (down).

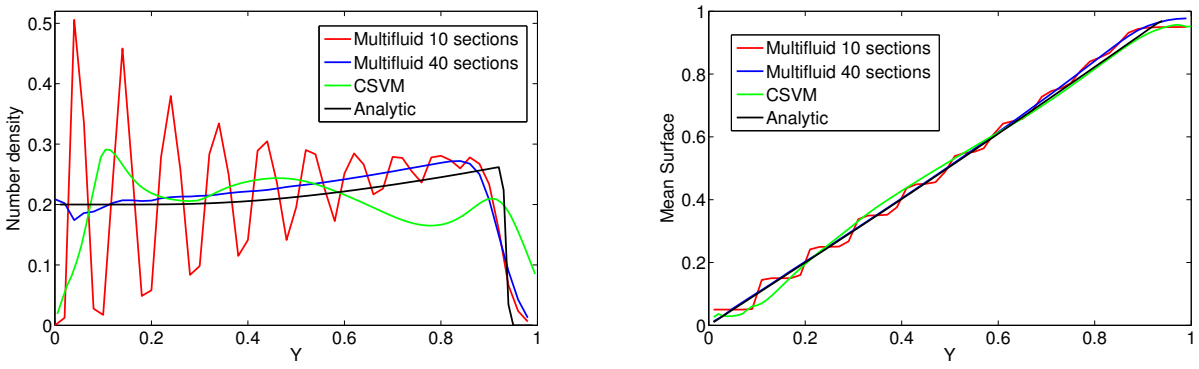

Figure 14: 2D Crossflow: droplet number density (left) and mean surface (right) at $X = 2$ against Y for the Multifluid approach with 10 sections (red line) and with 40 sections (blue line), the CSVM (green line) and the analytical solution (black line).

The initial number density distribution is :

$$n(r,t,S) = \frac{\sin(\pi W R)}{\pi W R} \tag{77}$$

$$R = \sqrt{(x-x_c)^2+(y-y_c)^2} \tag{78}$$

where $W = \sqrt{10}$ and $[x_c, y_c] = [0.275, 0.825]$. The size interval is $[0, 20St_c]$ where $St_c = 1/8\pi$. The initial droplet velocity is equal to the gas velocity. As no analycal solution was obtained a Lagrangian reference solution is proposed, the solver being described in Appendix 8.C.

On Fig. 15, the droplet number density and the mean surface for one section Multifluid, 40 sections Multifluid, lagrangian, and CSVM are shown at time $t = 1$. The one section solution shows the effect of a monokinetic assumption for the whole size distribution. Comparisons of the Lagrangian reference solution, the 40 sections Multifluid and the CSVM show a really good agreement. For the mean surface, the results of the CSVM are in really good agreement comparing the Lagrangian reference, and confirm the great accuracy of the method to capture the size-conditionned dynamics.

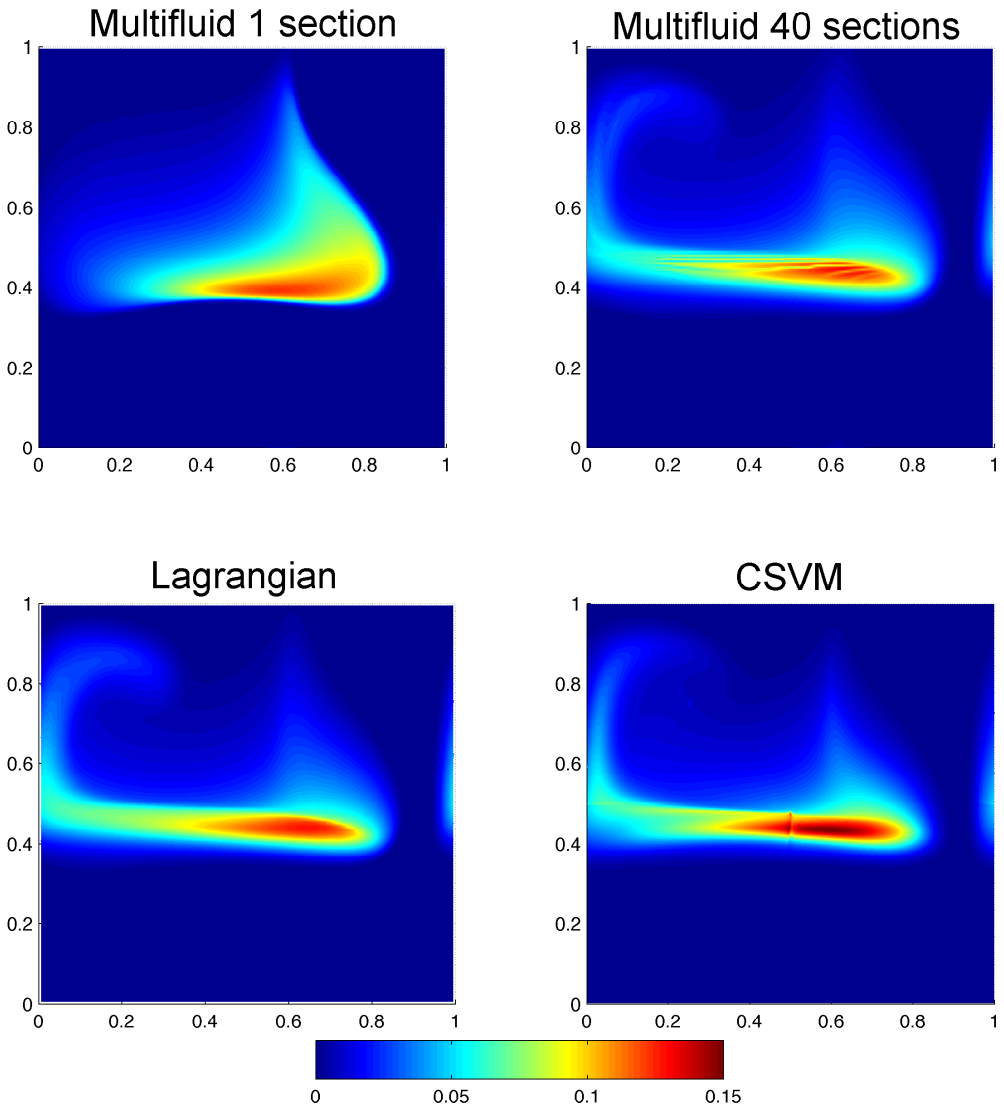

Figure 15: Taylor-Green vortices: droplet number density for the Multifluid approach with one section (upper left) and with 40 sections (upper right), the Lagrangian tracking with 10^8 particles, and the CSVM.

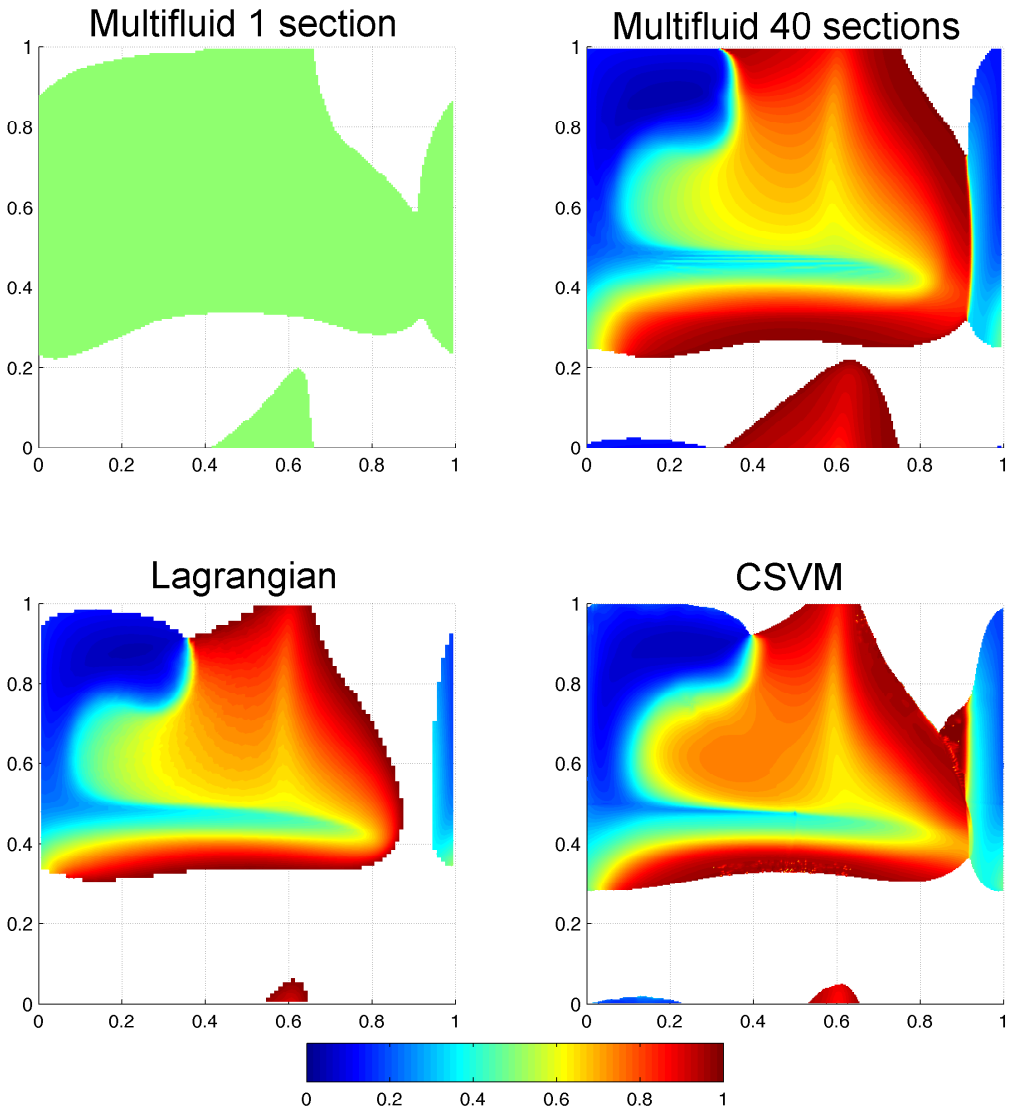

Figure 16: Taylor-Green vortices: mean surface for the Multifluid approach with one section (upper left) and with 40 sections (upper right), the Lagrangian tracking with 10^8 particles, and the CSVM.

7. Conclusions and outcomes

In this paper, the CSVM is proposed to account for size-velocity correlations, based on the EMSM of [13]. Basically, in the initial EMSM considered only one velocity for all sizes, which can lead to completely different dynamics for each size in the case of a wide spectrum of Stokes number for the particles. Moreover, this will also generate monodisperse distributions, which are difficult to reproduce using entropy maximization.

First, the entropy maximization is improved, in order to be able to reproduce size distributions close to the frontier of the moment space. Actually, the initial algorithm proposed in [13] is able to build NDF with canonical moments in $[0.01, 0.99]$. To cover a larger part of the moment space, a Gauss-Legendre method with an adaptive support is used, in such a way that quadrature points are used only where droplets lies. Furthermore, the Newton solver is optimized by adapting the number of parameters of the EM and by tabulating the initial guess.

Size-velocity correlations are accounted for, by using an additional moment in size-velocity for each direction. Using a power reconstruction and an equilibrium constraint for droplets of zero size ($U(S = 0) = U_g$), this allows to reconstruct the velocity for each size.

The evolution in phase space by drag force and evaporation is performed by evaluating the disappearance flux at zero size and the shift in size using a CQMOM quadrature. We emphasize on the fact that combining with a quadrature approach for the phase space evolution allows to use arbitrary evaporation and drag laws.

The evolution in physical space is done by using a flux splitting kinetic scheme, which separates positive and negative components of the fluxes to obtain an upwind scheme. By integrating this scheme over size, a realizable scheme is obtained, which is able to reproduce the proper dynamics of each size. This method is proved to be efficient on 1D cases.

Finally, the CSVM method is applied on two complex cases: the crossflow and the Taylor-Green vortices. Both cases are relatively well reproduced by the CSVM with only 8 moments, whereas the Multifluid approach need at least 40 moments to be efficient.

In future work, three issues will be investigated. The convection scheme need to be improved to reach high order, and reduce the numerical diffusion of such a first order scheme. The proposed formalism will be extended to turbulent dynamics, to be able to capture size-conditionned velocity dispersion induced by the turbulence. And a comparison of the computational time with Multifluid approaches in more realistic configuration (like injection configurations) has to be performed, as the highly segregative cases of the present work impose to reconstruct NDF at the frontier everywhere in the domain, increasing the computational cost due to the high number of iterations of the EM algorithm.

Acknowledgments

We would like to thanks Damien Kah for several helpful discussions and for providing numerous inputs and code sources from his Ph.D. Thesis where the EMSM was introduced. The motivation for the present study also stems from an original study of the crossflow configuration conducted in the Ph.D. Thesis of A. Vié as well as from discussions with his advisers S. Jay (IFPEN) and B. Cuenot (CERFACS), whom we take the occasion to thank here. The support from the RTRA DIGITEO as well as from Ecole Centrale Paris through the "Direction de la Recherche" for the Post-doctoral fellowship for A. Vié is gratefully acknolewdged. In fact the present study received a funding from this RTRA through the MUSE project (PI M. Massot - "MUltiscale Spray combustion fully Eulerian solver in 3D : a new generation of numerical methods and algorithms, high performance simulations, validation and visualization").

8. Appendix

8.A. Ability to capture Delta-Shock

Even if the proposed extension of the CSVM is able to capture the velocity associated with each size, it cannot capture the trajectory crossing for each size. Because the underlying semi-kinetic system is weakly hyperbolic, this will generate δ-shock. To evaluate the ability of the proposed method to capture accurately

δ-shock for each size, a 1D test case which is motivated by the Taylor-Green vortices is investigated. This configuration was further analysed in [25, 26].

In a 1D domain $[-\pi, \pi]$, a steady gas velocity field is set with $u_g = -\sin(x)$. Droplets are distributed uniformely at $t = 0$ with a null velocity and a constant droplet number density in size in the interval $[0, 20St_c]$. In this test case all trajectories meet at $x = 0$, generating a central δ-shock, which is fed by all sizes progressively.

On Fig. 17, droplet number density is plotted at different times. This confirm the ability of the scheme to capture δ-shock accurately. On Fig. 18, the comparison of the Multifluid with 1000 sections and the CSVM confirms the ability of the method to capture size-conditionned dynamics, even in the case of δ-shock.

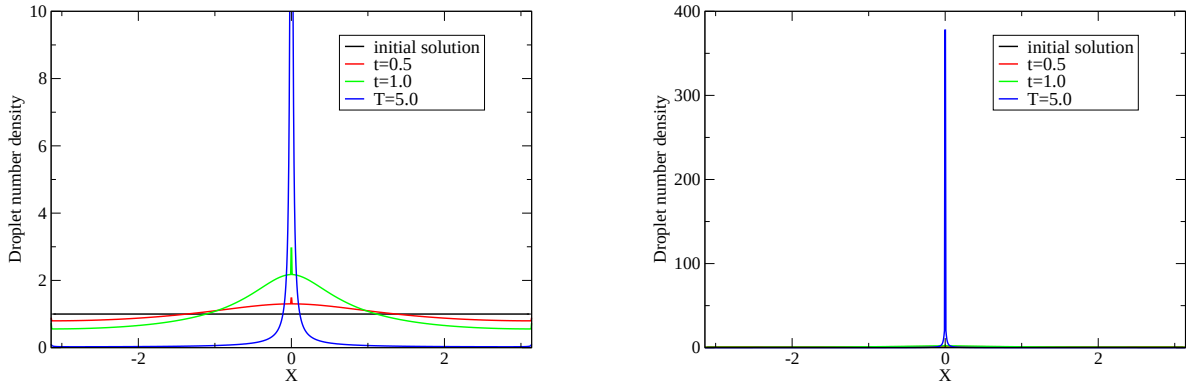

Figure 17: δ-shock generation: droplet number density zoomed on the initial solution (left) and at full scale (right) at time $t = 0$ (black line), $t = 0.5$ (red line), $t = 1.0$ (green line) and $t = 5.0$ (blue line)

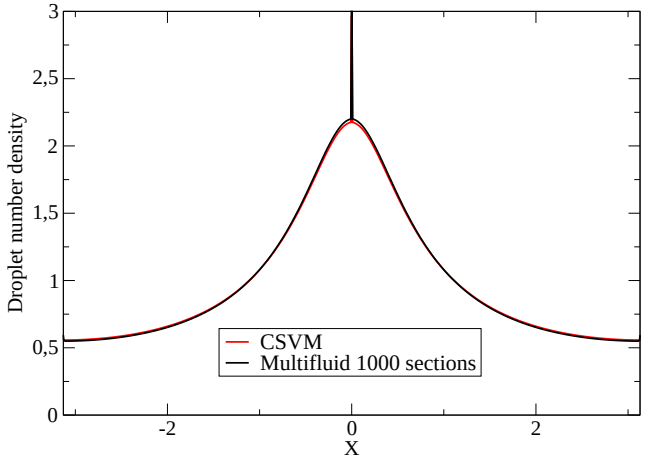

Figure 18: δ-shock generation: droplet number density at time $t = 1.0$ for CSVM (red line) and Multifluid with 1000 sections.

8.B. Semi-analytic solution for the 2D Crossflow

A semi-analytical solution is proposed, based on the solution for each size, and the fact that for one size, no droplet crossing occurs so that the lagrangian velocity is equal to the eulerian velocity $\vec{V_p}(t) = \vec{V}(t, X_p)$. Here we are looking for the solution against Y at a given position X.

Let $[X_p, Y_p]$ and $[U_p, V_p]$ be the position and the velocity of a particle, $[X_p^0, 0]$ and $[0, V^0]$ its initial position and velocity. Considering that $\vec{V_g} = U_g \vec{e_x}$:

$$\frac{dX_p}{dt} = U_p \quad , \quad \frac{dY_p}{dt} = V_p \tag{79}$$

$$\frac{dU_p}{dt} = \frac{U_p - U_g}{K_d S} \quad , \quad \frac{dV_p}{dt} = \frac{V_p}{K_d S} \tag{80}$$

So the lagrangian solution is:

$$U_p(t) = U_g \left(1 - \exp(-\frac{t}{K_d S})\right) \tag{81}$$

$$V_p(t) = V^0 \exp(-\frac{t}{K_d S}) \tag{82}$$

$$X_p(t) = X_p^0 + U_g \left(t + K_d S \left(\exp(-\frac{t}{K_d S}) - 1\right)\right) \tag{83}$$

$$Y_p(t) = V^0 K_d S \left(1 - \exp(-\frac{t}{K_d S})\right) \tag{84}$$

Y_p and V^0 do not depend on X_p^0, so V^0 is constant for a given Y. So the number density conservation gives that the droplet number density is constant on a vertical line between $X = X_{min}(Y)$ and $X = X_{max}(Y)$. The number density conservation equation is then:

$$\frac{\partial nV}{\partial Y} = = 0 \tag{85}$$

So the eulerian solution for droplet number density is:

$$n(Y) = \frac{n_{Y=0} V_0}{V(Y)} \tag{86}$$

Considering that eulerian and lagrangian velocity are equal at the same position:

$$t_Y = -K_d S \ln\left(1 - \frac{Y}{V^0 K_d S}\right) \tag{87}$$

$$V(Y) = V_p(Y_p(t_Y)) = V^0 \left(1 - \frac{Y}{V^0 K_d S}\right) \tag{88}$$

Finally:

$$n(Y, S) = \frac{n_{Y=0,S}}{\left(1 - \frac{Y}{V^0 K_d S}\right)} \text{ if } Y < V^0 K_d S \tag{89}$$

This solution is valid between Y_{min} and Y_{max} which depend on X. Considering non-dimensional coordinates $X_p^* = X_p / U_g K_d S$ and $Y_p^* = Y_p / V^0 K_d S$, the non dimensional trajectory of a particle is:

$$X_p^* = X_p^{0*} - \ln\left(1 - Y_p^*\right) - Y_p^* \tag{90}$$

and is plotted on Fig. 19.

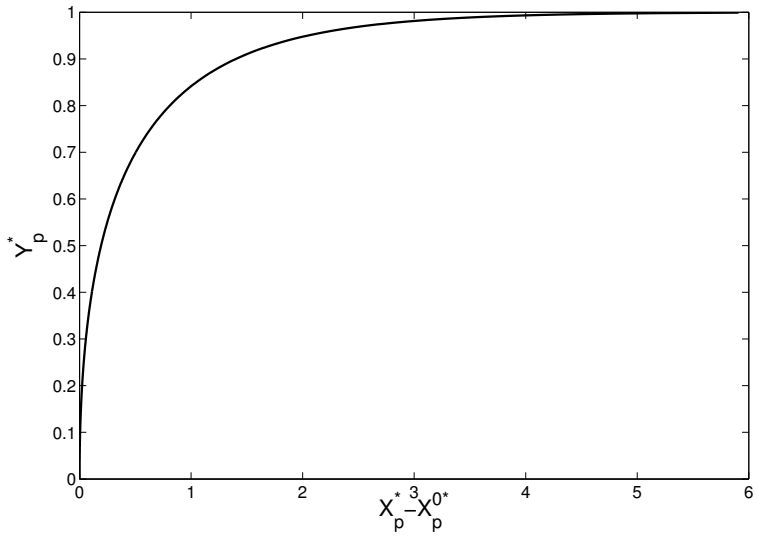

Figure 19: Non dimensional position

The injection is made between $X = X_L$ and $X = X_R$, which are respectively left and right limits. To check the solution, the mass conservation is examined:

$$\begin{aligned}\int_{Y_{min}}^{Y_{max}} n(Y)U(Y)dY &= \int_{X_L}^{X_R} n(Y=0)V^0 dX = n(Y=0)V^0(X_L - X_R) \\ &= n(Y=0)U_g\left[Y_{min} - Y_{max} - V^0 K_d S \ln\left(\frac{Y_{max} - V^0 K_d S}{Y_{min} - V^0 K_d S}\right)\right] \\ &= n(Y=0)V^0(X_L - X_R) \end{aligned} \tag{91}$$

which verify the mass conservation of the solution. The total droplet number density $n(Y)$ is obtained by integrating $n(Y,S)$ over all sizes and considering that only a size interval $[S_{min}(Y), S_{max}(Y)]$ can reach a given position Y:

$$n(Y) = \int_{S_{min(Y)}}^{S_{max}(Y)} n(Y,S)dS \tag{92}$$

S_{min} (resp. S_{max})corresponds to the droplet size for which the trajectory originating at X_L(resp. X_R) is equal to Y at the given X position:

$$S_{min}(Y) = \frac{Y}{V^0 K_d Y_p^*(X_L)} \tag{93}$$

$$S_{max}(Y) = \frac{Y}{V^0 K_d Y_p^*(X_R)} \tag{94}$$

$$\tag{95}$$

$$n(Y) = n(Y=0)\int_{S_{min(Y)}}^{S_{max}(Y)} \frac{1}{1 - \dfrac{Y}{V^0 K_d S}} dS \tag{96}$$

$$n(Y) = n(Y=0)\left[\frac{Y}{V^0 K_d}\ln\left(\frac{S_{max}(Y) - Y}{S_{min}(Y) - Y}\right) + S_{max}(Y) - S_{min}(Y)\right] \tag{97}$$

8.C. Lagrangian solution for Taylor-Green vortices

The reference solution for the Taylor-Green vortices is chosen to be a lagrangian computation, considering there is no analytical solution. This lagrangian computation consists in a discrete particle simulation with a sufficiently high number of particles to achieve converged statistics. The problem to solve is:

$$\begin{aligned} \frac{dX_p}{dt} = U_p \quad &, \quad \frac{dY_p}{dt} = V_p \\ \frac{dU_p}{dt} = -\frac{U_p - U_g}{K_d S} \quad &, \quad \frac{dV_p}{dt} = -\frac{V_p - V_g}{K_d S} \\ U_g = \cos(2\pi X_p)\sin(2\pi Y_p) \quad &, \quad V_g = -\sin(2\pi X_p)\cos(2\pi Y_p) \end{aligned}$$

for $p = 1, N_p$ where N_p is the number of particles. The initial number density distribution is a cardinal sinus in physical space $[0,1]^2$ and a constant distribution in size space $[0,1]$:

$$n(x,y,S) = \frac{\sin\left(\pi W\sqrt{(x-x_c)^2+(y-y_c)^2}\right)}{\pi W\sqrt{(x-x_c)^2+(y-y_c)^2}} \qquad \text{if} \quad \pi W\sqrt{(x-x_c)^2+(y-y_c)^2} \leq 1 \tag{98}$$

$$= 0 \qquad \text{if} \quad \pi W\sqrt{(x-x_c)^2+(y-y_c)^2} > 1 \tag{99}$$

where $[x_c, y_c]$ is the center of cardinal sinus distribution and W its width. To fulfill this distribution the rejection method is used. Using a uniform random number generator (here the native one of fortran), it allows to generate random numbers following any distribution. The random variable are the radius $r = \sqrt{x^2+y^2}$, the angle $\theta = \arctan\frac{y}{x}$, and the surface S. As the surface and angle distributions are constant, there is no need of the rejection algorithm for these variables. For the radius the random draw is made as follow:

1. Uniform random numbers r,θ,S and a test random number T are generated
2. if $r\max(n(r,S)) \geq T$ then the generated particle is conserved
3. if $r\max(n(r,S)) < T$ then the generated particle is rejected and a new particle is generated

This algorithm is reproduced until the required number of particles is reached. Then the lagrangian system of equation is solved in a semi-implicit manner. Here it is considered that during one time step, the gas velocity is constant. So one can derive an analytical solution for position and velocity:

$$U_p(t+\Delta t) = (U_p(t) - u_g(t))\exp\left(-\frac{\Delta t}{K_d S_p}\right) + u_g(t) \tag{100}$$

$$V_p(t+\Delta t) = (V_p(t) - v_g(t))\exp\left(-\frac{\Delta t}{K_d S_p}\right) + v_g(t) \tag{101}$$

$$X_p(t+\Delta t) = X_p(t) + u_g(t)\Delta t - K_d S_p(U_p(t) - U_g(t))\left(\exp\left(-\frac{\Delta t}{K_d S_p}\right) - 1\right) \tag{102}$$

$$Y_p(t+\Delta t) = Y_p(t) + v_g(t)\Delta t - K_d S_p(V_p(t) - V_g(t))\left(\exp\left(-\frac{\Delta t}{K_d S_p}\right) - 1\right) \tag{103}$$

In this approach, the only source of error is the variation of the gas velocity along the particle trajectory. The exact solution $U_p^e(t)$ is:

$$U_p^e(t+\Delta t) = U_p(t)\exp\left(-\frac{\Delta t}{K_d S_p}\right) + \int_0^{\Delta t}\frac{u_g}{K_d S}\exp\left(\frac{\tau - \Delta t}{K_d S_p}\right)d\tau \tag{104}$$

So the absolute error in this approach is:

$$|U_p^e(t+\Delta t) - U_p(t+\Delta t)| = \left| \int_0^{\Delta t} \frac{u_g}{K_d S} \exp\left(\frac{\tau - \Delta t}{K_d S_p}\right) d\tau \right| \quad (105)$$

$$\leq 2\pi \int_0^{\Delta t} \frac{\tau}{K_d S} \exp\left(\frac{\tau - \Delta t}{K_d S_p}\right) d\tau \quad (106)$$

$$\leq 2\pi \left(\Delta t - K_d S \left(1 - \exp\left(-\frac{\Delta t}{K_d S} \right) \right) \right) = \mathcal{O}(\Delta t^2) \quad (107)$$

So this method is second order in time and have the great advantage to be unconditionally stable comparing to the classical euler discretisation.

References

[1] L. Martinez, A. Benkenida, B. Cuenot, A model for the injection boundary conditions in the context of 3D simulation of diesel spray: methodology and validation, Fuel 89(1) (2010) 219–228.

[2] D. Kah, Taking into account polydispersity in the framework of a coupled Euler-Lagrange approach for the modeling of liquid fuel injection in internal combustion engines, Ph.D. thesis, Ecole Centrale de Paris, 2010. Available online at http://tel.archives-ouvertes.fr/tel-00618786/en/.

[3] A. Vié, S. Jay, B. Cuenot, M. Massot, Accounting for polydispersion in the eulerian large eddy simulation of an aeronautical-type configuration, To be submitted to Flow Turbulence and Combustion (2011).

[4] F. Doisneau, F. Laurent, A. Murrone, J. Dupays, M. Massot, Eulerian multi-fluid models for the simulation of dynamics and coalescence of particles in solid propellant combustion, Submitted to J. Comput. Phys. (2011). Available online at http://hal.archives-ouvertes.fr/hal-00618806/en.

[5] F. A. Williams, Spray combustion and atomization, Phys. Fluids 1 (1958) 541–545.

[6] F. A. Williams, Combustion Theory (Combustion Science and Engineering Series), ed F A Williams (Reading, MA: Addison-Wesley), 1985.

[7] G. A. Bird, Molecular gas dynamics and the direct simulation of gas flows, Oxford Science Publications 42 (1994).

[8] M. Garcia, Development and validation of the Euler-Lagrange formulation on a parralel and unstructured solver for large-eddy simulation, Ph.D. thesis, Université Toulouse III, 2009.

[9] A. Tagliani, Hausdorff moment problem and maximum entropy: a unified approach, Appl. Math. Comput. 105 (1999) 291–305.

[10] J. Greenberg, I. Silverman, Y. Tambour, On the origin of spray sectional conservation equations, Combustion and Flame 93 (1993) 90–96.

[11] F. Laurent, M. Massot, Multi-fluid modeling of laminar poly-dispersed spray flames: origin, assumptions and comparison of the sectional and sampling methods, Combust. Theory and Modelling 5 (2001) 537–572.

[12] J. Mossa, Extension polydisperse pour la description Euler-Euler des écoulements diphasiques réactifs, Ph.D. thesis, Institut National Polytechnique de Toulouse, 2005.

[13] M. Massot, F. Laurent, D. Kah, S. de Chaisemartin, A robust moment method for evaluation of the disappearance rate of evaporating sprays, SIAM J. Appl. Math. 70 (2010) 3203–3234.

[14] R. McGraw, Description of aerosol dynamics by the quadrature method of moments, Aerosol Science and Technology 27 (1997) 255–265.

[15] D. L. Marchisio, R. O. Fox, Solution of population balance equations using the direct quadrature method of moments, Journal of Aerosol Science 36 (2005) 43–73.

[16] F. Laurent, Numerical analysis of eulerian multi-fluid models in the context of kinetic formulations for dilute evaporating sprays, Mathematical Modeling and Numerical Analysis 3 (2006) 431–468.

[17] R. O. Fox, F. Laurent, M. Massot, Numerical simulation of spray coalescence in an eulerian framework: direct quadrature method of moments and multi-fluid method, Journal of Computational Physics 227 (2008) 3058–3088.

[18] L. R. Mead, N. Papanicolaou, Maximum entropy in the problem of moments, J. Math. Phys. 25 (1984) 2404–2417.

[19] H. Dette, W. J. Studden, The theory of canonical moments with applications in statistics, probability, and analysis, Wiley Series in Probability and Statistics: Applied Probability and Statistics, John Wiley & Sons Inc., New York, 1997. A Wiley-Interscience Publication.

[20] D. Kah, F. Laurent, M. Massot, S. Jay, A high order moment method simulating evaporation and advection of a polydisperse spray, In Press, J. Comput. Phys. (2011). Doi:10.1016/j.jcp.2011.08.032.

[21] D. L. Wright, Numerical advection of moments of the particle size distribution in Eulerian models, Journal of Aerosol Science 38 (2007) 352–369.

[22] C. Yuan, R. Fox, Conditional quadrature method of moments for kinetic equations, Journal of Computational Physics 230(22) (2011) 8216–8246.

[23] D. Wright, Numerical advection of moments of the particule size distribution in eulerian models, Journal of Aerosol Science 38(3) (2007) 352–369.

[24] J. Réveillon, C. Péra, M. Massot, R. Knikker, Eulerian analysis of the dispersion of evaporating polydispersed sprays in a statistically stationary turbulent flow, Journal of Turbulence 5 (2004) 1–27.
[25] M. Massot, "Eulerian multi-fluid models for polydisperse evaporating sprays", CISM Courses and Lectures, Springer Wien, R.O. Fox et D. Marchisio Eds.
[26] M. Massot, F. Laurent, S. de Chaisemartin, L. Fréret, D. Kah, Eulerian multi-fluid models: modeling and numerical methods, in: Modelling and Computation of Nanoparticles in Fluid Flows, Lectures Notes of the von Karman Institute, NATO RTO-EN-AVT-169, 2009. Available online at http://hal.archives-ouvertes.fr/hal-00423031/en/.